South African Journal of Botany 130 (2020) 282–299

Contents lists available at ScienceDirect

South African Journal of Botany

journal homepage: www.elsevier.com/locate/sajb

Sesbania grandiflora L. Poir leaves: A dietary supplement to alleviate type 2 diabetes through metabolic enzymes inhibition

Bathini Thissera[a], Rizliya Visvanathan[b], Mohammad A. Khanfar[c,d], M. Mallique Qader[a,b], Marwa H.A. Hassan[e], Hossam M. Hassan[e], Majed Bawazeer[a], Fathy A. Behery[f,g], Mohammed Yaseen[a], Ruvini Liyanage[b], Usama R. Abdelmohsen[h,i,*], Mostafa E. Rateb[a,**]

[a] School of Computing, Engineering & Physical Sciences, University of the West of Scotland, Paisley PA1 2BE, Scotland, UK
[b] National Institute of Fundamental Studies, Hantana Road, Kandy, Sri Lanka
[c] Faculty of Pharmacy, The University of Jordan, Amman, Jordan
[d] College of Pharmacy, Alfaisal University, Al Takhassusi Road, Riyadh, Saudi Arabia
[e] Department of Pharmacognosy, Faculty of Pharmacy, Beni-Suef University, Beni-Suef 62514, Egypt
[f] Department of Pharmacognosy, Faculty of Pharmacy, Mansoura University, Mansoura 35516, Egypt
[g] Department of Pharmaceutical Sciences, College of Pharmacy, Riyadh Elm University, Riyadh, Saudi Arabia
[h] Department of Pharmacognosy, Faculty of Pharmacy, Minia University, Minia 61519, Egypt
[i] Department of Pharmacognosy, Faculty of Pharmacy, Deraya University, 61111 New Minia, Egypt

ARTICLE INFO

Article History:
Received 29 August 2019
Revised 28 December 2019
Accepted 7 January 2020
Available online xxx

Edited by V Kumar

Keywords:
Loliolide
Quercetin
Sesbania grandiflora
Vomifoliol
A-amylase
A-glucosidase

ABSTRACT

Sesbania grandiflora L. Poir is an edible medicinal plant widely distributed in Asian countries. One of its folk medicinal uses is the alleviation or treatment of Type 2 Diabetes mellitus (T2DM). A number of animal studies confirmed its use in treating T2DM; however, none of them explored the chemistry or the possible mechanism. This study aims to unveil the chemical profile of *S. grandiflora* through LC-HRMS dereplication analysis, followed by isolation, identification and quantification of the major secondary metabolites with potential α-amylase and α glucosidase inhibitory effect as the potential anti-diabetic mechanism. LC-HRMS chemical profiling of its leaves and twigs identified 32 metabolites. Bio-guided fractionation and HPLC purification led to the isolation of 14 major metabolites that were screened for their α-amylase and α-glucosidase inhibitory activities. For the first time, two terpenoids; vomifoliol **(11)** and loliolide **(14)** showed inhibitory effect against α-glucosidase with IC_{50} values of 64.5 and 388.48 μM, respectively. Quercetin **(10)** exhibited the highest α-glucosidase inhibition with IC_{50} value of 17.45 μM. Further, predicated molecular modelling studies demonstrated strong binding interactions between active compounds and enzyme-substrate binding pockets supporting the observed enzyme inhibitory activity. Interestingly, the quantitative analysis of the most potent inhibitors indicated their existence at a high percentage within *S. grandiflora* extract. Our findings suggested *S. grandiflora* is a useful dietary supplement to control postprandial blood glucose.

1. Introduction

Diabetes mellitus (DM) is a metabolic disease caused by various factors and mainly characterised by high blood glucose levels medically termed as hyperglycaemia (Kwon et al., 2008; Li et al., 2019). DM is usually associated with other critical complications like diabetic neuropathy, high blood pressure, obesity and cardiovascular diseases, etc. More than 90% of diabetes cases were reported as T2DM, which is characterised by impaired insulin secretion by pancreatic β-cells or disorders associated with carbohydrate, lipid and protein metabolism. Among various factors, the fast uptake of glucose resulted from the breaking down of polysaccharides by α-amylase and α-glucosidase influence homeostasis. As the significant importance of these two enzymes, they are being targeted during the invention of new drug therapies against T2DM (Dong et al., 2012; Oboh et al., 2012). However, current treatments which are showing inhibitory action against these two enzymes such as acarbose are present with various side effects, such as the distended abdomen, diarrhoea, flatulence, constipation which cause poor patient compliance (Li et al., 2019).

Abbreviations. T2DM, Type 2 Diabetes mellitus; NMR, Nuclear Magnetic Resonance; LC-HRMS, Liquid Chromatography-High Resolution Mass Spectroscopy; HPLC, High Pressure Liquid Chromatography; MeEx, Methanolic extract; MeCN, Acetonitrile; MeOH, Methanol; SMs, Secondary metabolites

* Corresponding author at: Department of Pharmacognosy, Faculty of Pharmacy, Minia University, Minia 61519, Egypt.
** Corresponding author at: School of Computing, Engineering & Physical Sciences, University of the West of Scotland, Paisley, PA1 eBE, Scotland, UK
E-mail addresses: usama.ramadan@mu.edu.eg (U.R. Abdelmohsen), Mostafa.Rateb@uws.ac.uk (M.E. Rateb).

https://doi.org/10.1016/j.sajb.2020.01.011
0254-6299/

There is an increasing demand for naturally occurring secondary metabolites as therapeutic agents, and this trend is rationalized by their proven biocompatibility and better patient compliance (Talapatra and Talapatra, 2015). In fact, natural products have biological origin associated with the evolutionary optimised properties to complement biological activities. For example, binding with specific target proteins or other biomolecules reflects their potential suitability as viable drug agents (Atanasov et al., 2015). *Sesbania grandiflora* (L.) Poir. belongs to the family Fabaceae, known as "Agathi" in India and "Kathurumurunga" in Sri Lankans, although it is native to Sri Lanka, India, Australia, Indonesia, Malaysia, Myanmar and the Philippines (Balasuriya and Dharmaratne, 2007); Munde-Wagh et al., 2012). Various parts of *S. grandiflora* have been reported to have antibacterial, antifungal, antioxidant, anti-diabetic, anti-inflammatory and antitumor properties (Das, et al., 2013; Goun et al., 2003; Laladhas et al., 2008; Shareef et al., 2012). In traditional systems of medicine, the whole plant of *S. grandiflora* is used to treat various types of ailments, such as bacterial infections, inflammation, fever, rheumatic swellings, ulcers, nasal catarrh, nyctalopia, cephalalgia, febrifuge, diarrhoea, gastralgia, dyspepsia, and to cure scabies (Roy et al., 2014; Wagh et al., 2009). Aqueous suspension of *S. grandiflora* leaves significantly decreased the elevated hepatic, renal and lipid peroxidation markers and ameliorated the diminished antioxidant levels in cigarette smoke-exposed rats, restored brain oxidative damage, showed a potential cardioprotective effect in cigarette smoke-induced rats by protecting the heart from oxidative stress (Ramesh et al., 2008, 2010, 2015). A recent ethnobotanical survey carried out in the Eastern province of Sri Lanka revealed the use of *S. grandiflora* leaves as a Siddha medicine to treat diabetes (Sathasivampillai et al., 2018). The anti-diabetic nature of *S. grandiflora* leaves was confirmed when methanolic extract of the leaves (200 and 400 mg/kg, p.o.), and the standard drug, metformin (10 mg/kg), administered for 28 days induced significant reduction of elevated blood glucose levels in type 2 diabetic rats induced by low dose streptozotocin and high-fat diet (Panigrahi et al., 2016). Administration of methanolic extract of *S. grandiflora* flowers, with glibenclamide as drug control, for 45 days to streptozotocin-induced diabetic rats resulted in the reduction of blood glucose and glycosylated haemoglobin levels with increased levels of insulin and haemoglobin. Moreover, the extract reversed the protein and lipid peroxidation markers, osmotic fragility, membrane-bound ATPases activities, and antioxidant status in streptozotocin-induced diabetic rats (Sureka et al., 2015). Additionally, the anti-diabetic nature of *S. grandiflora* seeds was proven by treating streptozotocin-induced diabetic mice with aqueous extract of its seeds. Administration of 2.5 g/Kg body weight was able to lower the initial blood glucose level from 435 to 213 mg/dL within 18 days of treatment (Zamroni et al., 2017). The methanol extract of *S. grandiflora* seeds that contained derivatives of piperidine, cinnamaldehyde and linolenic acid showed significant inhibition of α-amylase (52%) and α-glucosidase (56%) (Prasanna and Saraswathi, 2013). The flower decoction of *S. grandiflora*, rich in chlorogenic and neochlorogenic acids, showed moderate α-amylase and α-glucosidase inhibitory activities in addition to a strong antioxidant effect (Baessa et al., 2019).

Few previous studies highlighted the chemical composition in *S. grandiflora*. GC–MS analysis of methanol extract of the leaves of *S. grandiflora* indicated the presence of 3,4,5-trimethoxyphenol, erucic acid, 2-furancarboxaldehyde, vitamin E acetate, 4-methyloxazole, palmitic acid, and 9-hexadecenol (Hussain and Kumaresan 2014). Total phenolic profiling of *S. grandiflora* leaves methanolic extract showed high phenolic contents of quercetin and kaempferol (Mustafa et al., 2010). Additionally, the isoflavonoids isovesitol, medicarpin, sativan together with the lupine triterpene betulinic acid were recently isolated from roots of *S. grandiflora* and showed good inhibitory activity against *Mycobacterium tuberculosis* (Hasan et al., 2012). A recent study conducted by Anantaworasakul et al., 2017, suggested that the fractionated extracts of *S. grandiflora* bark contained antioxidant and antibacterial activities which could be related to the high content of gallic acid based on HPLC analysis.

Though the curative properties are known and proven, the full chemical profiling of this plant species is still understudied. Therefore, this study aimed to use the dereplication-based LC-HRMS analysis to unveil the chemical profile of *S. grandiflora* crude extract of leaves and twigs to rationalise its medicinal properties in folk medicine including the antidiabetic effect of its total extract in animal models. Herein, we have studied the chemical profile of the methanolic extract of leaves and twigs of *S. grandiflora* utilising LC-HRMS analysis to investigate the ability of *S. grandiflora* to produce secondary metabolites and their diversity for the first time. Based on the overall evaluation of chemical compounds with the aid of published literature and their reported biological properties, chemical analysis was performed followed by extraction, purification, isolation and structure characterisations. Fourteen known secondary metabolites belonging to flavonoids and terpenoids were isolated by RP-HPLC and characterised by NMR and LC-HRMS. The inhibitory activities of these compounds against α-amylase and α-glucosidase enzymes were evaluated using *in vitro* and computational molecular modelling experiments. Apart from the anti-diabetic action and antioxidant potential of the crude extracts, the isolated pure compounds were also studied. The formation of reactive oxygen species (ROS) is increased by DM and associated with oxidative stress mainly through oxidation, nonenzymatic protein glycation, and oxidative degradation of glycated proteins. Therefore, the ability of anti-diabetic therapies to scavenge ROS would be an added advantage to prevent vascular complications in diabetes (Johansen et al., 2005).

2. Materials and methods

2.1. Chemicals

All solvents used for analytical purposes were purchased from Fisher Chemical UK, and all HPLC grade solvents were from Rathburn Chemicals Ltd UK. Thin layer chromatography (TLC) technique was used for preliminary identification and performed on silica gel coated with fluorescent indicator plates purchased from Macherey-Nagel, Germany and visualised under UVGL Handheld UV lamp. The reference compounds for quantitative analysis, the internal standard (IS) 4-hydroxycinnamic acid (99%), quercetin (98%) and kaempferol (98%) were purchased from Sigma Aldrich, UK, while vomifoliol and loliolide were isolated from *S. grandiflora* with >95% purity.

2.2. Instruments

Agilent 1100 series HPLC system connected to Diode Array Detector (serial Number DE03010630) was utilised for purification. HRESIMS data were obtained using a Thermo LTQ Orbitrap coupled to HPLC system (PDA detector, PDA autosampler, and pump). Structure characterisation of all the compounds was based on ^{1}H NMR, ^{13}C NMR, COSY, HSQC, and HMBC data, using Bruker Avance III spectrometer 600 MHz.

2.3. Plant material

Leaves and twigs of *S. grandiflora* ware collected from Central province of Sri Lanka in April 2016. Dr M.N. Napagoda, University of Ruhuna, Sri Lanka, authenticated the plant. Voucher specimen with code (BTSG-7022015) was deposited at the School of Computing, Engineering and Physical Sciences, University of the West of Scotland, Paisley, UK.

2.4. Extraction

The shade dried plant material was powdered using a mechanical grinder (Kenwood 350 W). About 650 g powder material was extracted with methanol and acetone (2 L each) under sonication. The methanol extract was dried under vacuum to produce a crude extract (50.8 g) as a dark green gummy residue. To remove the chlorophylls, the crude extract was re-dissolved in 80% of aqueous methanol followed by refrigeration overnight and the precipitate formed was removed by filtration. The filtrate was evaporated under vacuum. Resulted total extract was defatted by shaking with hexane.

2.5. Preparation of samples and LC-HRMS analysis

For LC-MS analysis, 1 mg of the defatted methanolic extract of *S. grandiflora* was accurately weighed and dissolved in 10 mL of methanol, and about 1 mL of this solution was filtered through 0.2 μm PTFE filter (Milian, Geneva, Switzerland) into HPLC vial and submitted to LC-HRMS analysis in triplicate together with methanol as the solvent blank.

HRESIMS data were obtained using a Thermo LTQ Orbitrap coupled to an HPLC system (PDA detector, PDA autosampler, and pump). The following conditions were used: capillary voltage of 45 V, capillary temperature of 260 °C, auxiliary gas flow rate of 10–20 arbitrary units, sheath gas flow rate of 40–50 arbitrary units, spray voltage of 4.5 kV, and mass range of 100–2000 amu (maximal resolution of 30,000). For MS detection, ionisation was performed in positive and low-resolution negative ESI modes using a mass scan range from 85 to 1000 Da.

2.6. HRMS data processing with MZmine 2.37

Raw mass data files obtained from LC-HRMS were sliced into two data sets as positive and negative based on ionisation mode using MassConvert tool from Proteo Wizard. As the negative mode was not high resolution, only positive mode files were considered for further process. The sliced positive mode data files of all triplicate samples of the methanolic extract and the methanol blank were imported and processed using MZmine 2.37 software following the steps, and predefined parameters explained in Macintyre et al. (2014). The sequence of steps involved are peak detection (mass detection and chromatogram builder), chromatogram deconvolution, deisotoping, filtering, alignment, gap filling, adduct and complex ion search and finally formula prediction. Final data output from the MZmine 2.37 was exported to CSV file, and further clean-up was done manually by removing adducts and peaks present in both samples and solvent blank as explained in Macintyre et al., 2014. Additionally, the formulae which did not follow the nitrogen rule were also eliminated. Predicted formulae and respective retention times in the CSV file were further checked with Xcalibur 3.1 software predictions using raw mass data files to eliminate unreliable formulae and cross-checked the unidentified peaks by MZmine for their accuracy.

2.7. The process of dereplication to identify known and new hits

After the clean-up process, the CSV file was aligned into ascending order with the peak retention times. Predicted formulae were searched using SciFinder, Dictionary of Natural product Ver. 26.1, DEREP-NP 2015 and Reaxys online databases. This was followed by a thorough search of the fragmentation patterns of the precursor ion on Xcalibur 4.1 with the aid of fragmentation tool available with ChemDraw professional 17.0 (PerkinElmer Informatics, Cambridge, UK) to make lists of best possible hits. The tentatively identified and un-identified hits were subjected to a literature survey of their biology (Table 1).

2.8. Isolation and structure characterisation

The total defatted extract (41.5 g) was subjected to vacuum liquid chromatography (VLC) yielding eight fractions (Fr1-Fr8). VLC was run on a silica gel column using DCM/MeOH (1:0/0.1, v/v) with a 5% gradient of MeOH at each 200 mL of solvent. Each fraction was screened on TLC using different solvent systems and the fractions which were found to be similar (Fr 1–3), and Fr (5–6) combined to produce three subfractions named Fr_1, Fr_2 and Fr_3. Purification of Fr_1 by HPLC (Phenomex C18, 250 × 10 mm, 5 μm) using CH_3CN-water (20% → 60% CH_3CN for 30 min, 75% → 100% CH_3CN for another 10 min, total of 40 min run) eluted compounds: **8** (t_R17.2 min, 2 mg), **9** (t_R18.0 min, 9 mg) and **10** (t_R14.4 min, 10 mg). Furthermore, Fr_2 was purified by reversed-phase HPLC (Phenomenx C18, 250 × 10 mm, 5 μm) eluted with H_2O–CH_3CN (25% →75% CH_3CN for 20 min, 75% →100% CH_3CN for 5 min, total of 25 min run) to afford compounds: **2** (t_R 8.5 min, 7 mg), **3** (t_R 9.1 min, 10 mg), **4** (t_R 11.6 min, 1.5 mg), **5** (t_R 9.6 min, 2 mg), **6** (t_R 10.2 min, 4 mg) and **7** (t_R 12.6 min, 9 mg). Fr_3 was also purified on semi-preparative HPLC using reversed-phase C18 column (Sunfire™, 250 × 10 mm), eluted with H_2O–CH_3CN (25% →100% CH_3CN for 30 min, 100% CH_3CN for 5 min, total of 35 min run) to furnish compounds **1** (t_R 25.2 min, 4 mg), **11** (t_R 11.7 min, 10 mg), **12** (t_R 14.3 min, 3 mg), **13** (t_R 9.1 min, 3 mg) and **14** (t_R 15.2 min, 4 mg).

2.9. α-Amylase inhibitory activity

The α-amylase inhibitory activity was determined using the method described by Visvanathan et al., 2016. The assay system comprised the following components in a total volume of 260 μL: 40 μL of PBS (0.02 M, pH 6.9), 100 μL of GOD/POD reagent, with 40 μL of each soluble starch (2 g L^{-1}), inhibitor solution (*S. grandiflora* MeEx, fractions and pure compounds) and the enzyme solution (15 Unit mL^{-1}). Briefly, the enzyme solution was mixed with the inhibitor solution and pre-incubated on a hotplate for 10 min at 37 °C. The reaction was started by pipetting the soluble starch solution into each well containing pre-incubated enzyme solution mixed with the plant metabolites, and the content was incubated for another 15 min. Finally, 100 μL of the GOD/POD reagent was added, and the absorbance was measured at 505 nm after 15 min using the Thermo Scientific Multiskan GO Microplate Reader. PBS (40 μL) was used as a negative control, and the absorbance was measured parallel with samples.

2.10. α-Glucosidase inhibitory activity

α-Glucosidase inhibitory activity was determined according to the method of Liyanage et al. (2018) with minor modifications. The effect of the *S. grandiflora* MeEx, fractions and pure compounds on yeast-derived α-glucosidase enzyme was determined by using p-nitrophenylglucopyranoside (pNPG) as the substrate. First, 100 μL of phosphate buffer (pH 6.9, 0.1 M), 20 μL of plant metabolites, and 50 μL of α-glucosidase enzyme (0.4 Unit mL^{-1}) were added into a 96 well plate and incubated for 15 min at 37 °C. Next, 50 μL of pNPG was added into the wells, and the content was incubated for another 30 min at 37 °C. Finally, the absorbance was taken at 400 nm, and the results were expressed in terms of IC_{50} value.

2.11. ABTS radical scavenging assay

The ABTS free radical-scavenging activity was determined according to the method described by Tupe et al., 2013 with minor modifications. A mixture of ABTS (2.5 mM) and potassium persulfate (2.0 mM) was allowed to stand overnight at room temperature in the dark for the formation of the ABTS radical cation. The $ABTS^+$ solution was then diluted with PBS buffer (5 mM, pH 7.4) to obtain a control absorbance of 0.70 ± 0.005 at 734 nm. A volume of 50 μL of each sample stock was added to a 96-well plate followed by the addition

Table 1
Compounds identified in MeEx by LC-HRESIMS analysis.

Rt (min)	m/z $[M+H]^+$	Molecular formula	Tentative identification	Structure	Bioactivity	Reference
4.98	741.2223	$C_{33}H_{40}O_{19}$	Kaempferol−3−2G- rhamnosyl-rutinoside	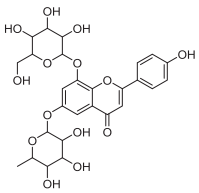	Anti-inflammatory activity	Eom et al. (2016)
5.69	611.1597	$C_{27}H_{30}O_{16}$	Kaempferol-3-O-β-D-glucopyranosyl-(1→2)-β-D-galactopyranoside	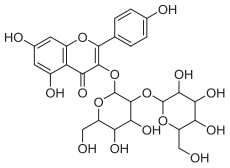	Significant anti-diabetic activity as an α-amylase inhibitor	Milella et al. (2016)
6.02	595.1643	$C_{27}H_{30}O_{15}$	Kaempferol-3-O-(6"-α- rhamnopyranosyl)-β- glucopyranoside	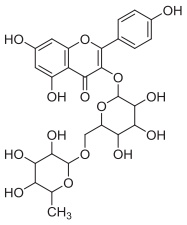	Antioxidant and anti-inflammatory. Inhibitory activity against advanced glycation end-product formation	Chen et al. (2019), Sato et al. (2017)
6.24	237.1861	$C_{15}H_{24}O_2$	Carisone	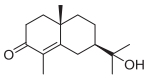	Bioactivity not reported	Achenbach et al. (1985)
6.49	371.2081	$C_{19}H_{30}O_7$	7-megastigmadien-3-one-9-O-β-D-glucopyranoside	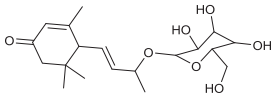	Influenza neuraminidase inhibitor	Liu et al. (2016)
6.55	449.1085	$C_{21}H_{20}O_{11}$	Astragalin	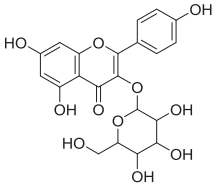	Potent treatment for diabetic testicular function impairment, Anti-bacterial and anti-inflammatory	Han et al. (2019), Frezza et al. (2018)
6.95	419.0977	$C_{20}H_{18}O_{10}$	Keampferol-5-O-arabinoside	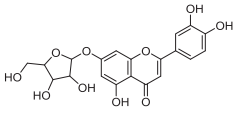	Antioxidant and anti-inflammatory activities	Galasso et al. (2014)
7.44	933.2658	$C_{43}H_{48}O_{23}$	Astraflavonoid B	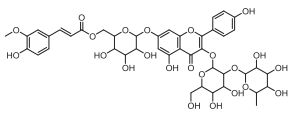	Bioactivity not reported	Hao et al. (2016)
7.50	477.1384	$C_{23}H_{24}O_{11}$	Luteolin-7-O-β-glucopyranoside	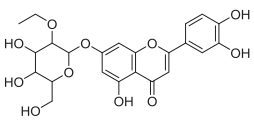	Antioxidant and moderate cytotoxic activity	Al-Qudah et al. (2017)

(*continued*)

Table 1 (*Continued*)

Rt (min)	*m/z* $[M+H]^+$	Molecular formula	Tentative identification	Structure	Bioactivity	Reference
7.72	917.2686	$C_{43}H_{49}O_{22}$	Choushenoside A	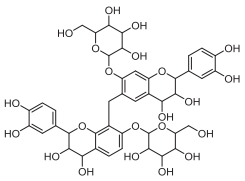	Bioactivity not reported	Qin et al. (2018)
8.37	695.2185	$C_{32}H_{38}O_{17}$	3, 6′-di-O-feruloylsucrose	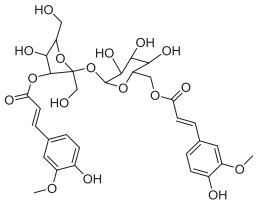	Bioactivity not reported	Choudhary et al. (2006)
8.50	303.0518	$C_{15}H_{10}O_7$	Quercetin	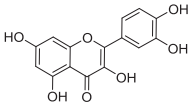	Antidiabetic and antioxidant agent	Sarian et al. (2017)
8.65	845.2501	$C_{40}H_{44}O_{20}$	Scarbroside	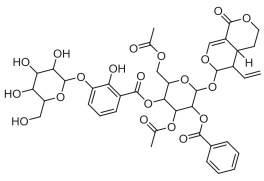	Strong anti-inflammatory activity	Wang et al. (2013)
8.88	699.1924	$C_{34}H_{34}O_{16}$	Tricin 7-O-(600-(*E*)-sinapoyl)-*β*-D-glucopyranoside	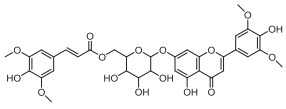	No activity reported	
9.30	285.1714	$C_{15}H_{24}O_5$	(6*S*,7*E*)−6,9-dihydroxy-10-(2′-hydroxyethoxy)−4,7-megastigmadien-3-one	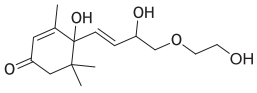	Antioxidant and anti-inflammatory activity	Yang et al. (2016)
9.57	293.2129	$C_{18}H_{28}O_3$	Kolavonic acid	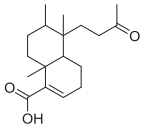	Bioactivity not reported	Pereira et al. (2012)
9.57	465.3198	$C_{21}H_{20}O_{12}$	Isoquercitrin	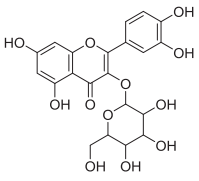	Bioactivity not reported	Luo et al. (2016)
9.66	287.0468	$C_{15}H_{10}O_6$	Kaempferol	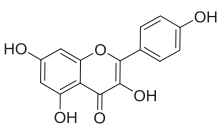	Antibacterial and anxiolytic effect. Significant *α*-amylase inhibitor	Frezza et al. (2018), Milella et al. (2016)

(*continued*)

Table 1 (*Continued*)

Rt (min)	m/z $[M+H]^+$	Molecular formula	Tentative identification	Structure	Bioactivity	Reference
9.81	235.1706	$C_{15}H_{22}O_2$	Callitrin	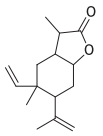	Antidiabetic and antioxidant agent	Sarian et al. (2017)
10.13	287.1297	$C_{17}H_{18}O_4$	Dendroinfundin A	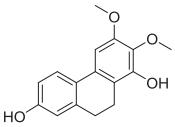	No antidiabetic activity	Na Ranong et al. (2018)
11.49	225.1412	$C_{13}H_{20}O_3$	Vamifoliol	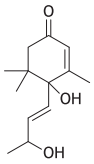	Bioactivity not reported	Macías et al. (2004)
12.04	209.1463	$C_{13}H_{20}O_2$	megastigmane 3-oxo-α-ionol	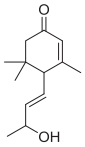	Bioactivity not reported	Macías et al. (2004)
12.25	301.0636	$C_{16}H_{12}O_6$	Rhamnocitrin	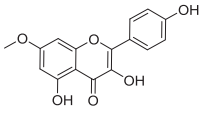	A potent anti-tumour activity	Baek et al. (2019)
12.65	243.1612	$C_{13}H_{22}O_4$	3,5,6-trihydroxy-7-megastigmen-9-one	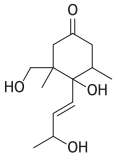	Anti-ageing and anti-inflammatory activity	Park et al. (2011), Chen et al. (2019)
13.19	335.1777	$C_{19}H_{26}O_5$	8β-isobutyryloxy cumambranolide	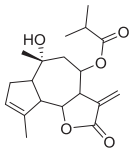	Bioactivity not reported	Kuo et al. (1998)
13.25	283.0985	$C_{17}H_{14}O_4$	Chrysin-dimethylether	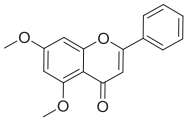	A potent breast cancer inhibitor. CYP3A4 enzyme inhibitor.	Bae et al. (2018), Šarić Mustapić et al. (2018)
13.81	287.1209	$C_{17}H_{18}O_4$	Sativan	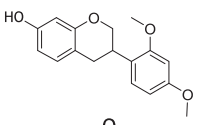	Antituberculotic action	Hasan et al. (2012)
15.20	196.1231	$C_{11}H_{16}O_3$	Loliolide	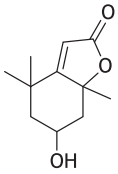	Antidiarrheal, antibacterial, anti-inflammatory, anthelmintic	Adnan et al. (2019)

(*continued*)

Table 1 (*Continued*)

Rt (min)	*m/z* $[M+H]^+$	Molecular formula	Tentative identification	Structure	Bioactivity	Reference
16.13	347.2211	$C_{21}H_{31}O_4$	pachyclavulariolides D	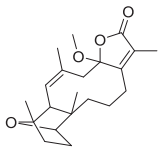	Bioactivity not reported	Xu et al. (2000)
18.76	413.2672	$C_{21}H_{32}O_8$	11-O-β-D-glucopyranoside-abscisic alcohol	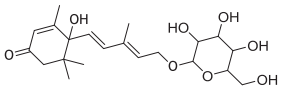	Bioactivity not reported	Lutz and Winterhalter (1992)
19.39	367.1679	$C_{19}H_{26}O_7$	Britanin	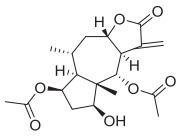	Bioactivity not reported	Whazin et al. (1995)
20.86	387.2022	$C_{19}H_{30}O_8$	Sonchuionoside A	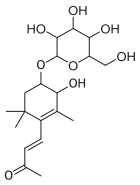	Bioactivity not reported	Shimizu et al. (1989)

of 200 μL $ABTS^+$ solution. Finally, the absorbance was measured at 734 nm after 6 min incubation at room temperature. Test results were expressed as mM Trolox equivalents per gram of crude sample (DW).

2.12. Quantitative analysis of the most potent enzyme inhibitors

2.12.1. Preparation of sample and stock solutions

Four standard solutions of compound **9, 10, 11** and **14** were prepared in 250 ppm concentration by accurately weighing 1 mg of each compound and dissolving in MeOH using a 5 mL volumetric flask. Each solution was vortexed for 2 min and serially diluted in methanol to prepare a series of six concentrations from 125 ppm to 4 ppm. Then, 4-hydroxycinnamic (4-CA) acid, which is structurally similar to 2-hydroxycinnamic acid, was used as the internal standard (IS). However, this was reported as a specific IS for phenolic acid and flavonoid quantification by Lin et al. (2015). Standard of 100 ppm solution of IS was prepared by dissolving accurately weighed 0.5 mg of 4-CA in 5 mL of methanol. 100 μL of IS was added in each concentration in the series. 10 mg of MeEX of *S. grandiflora* was dissolved in 10 mL of methanol and centrifuged at 5000 rpm for 10 min. Then, 1 mL of the supernatant was filtered through 0.2 μm PTFE filter (Milian, Geneva, Switzerland) into HPLC vial. The sample solution was also added with 100 μL of IS.

2.12.2. Optimization of chromatographic conditions

Chromatographic analysis was performed on Agilent 1100 series HPLC system connected to Diode Array Detector (serial number DE03010630). Few attempts to develop and optimise a chromatographic method to produce a chromatogram with a good peak resolution for the total MeEx of *S. grandiflora* using different columns, solvent systems and parameters were applied. Consequently, the most acceptable chromatogram for the MeEx of *S. grandiflora* was achieved on Phenomenx C18 analytical column (250 × 4.60 mm) (Fig. 4) with CH_3CN/H_2O (0% →30% CH_3CN for 20 min, 30% →80% CH_3CN for 10 min). The flow rate was kept constant at 0.80 mL/min, the optimised injection volume was at 5 μL and system temperature was set to 25 °C. The chromatogram was recorded at a wavelength of 254 nm.

2.12.3. Calibration curves and quantification

Four calibration curves for compounds **9, 10, 11** and **14** were plotted with six concentrations of standard solutions. Each concentration in the series was injected into the HPLC individually in triplicate under the same chromatographic conditions to produce the chromatogram for the total MeEx of *S. grandiflora*. The Curves were constructed by the peak area ratio of the standard solutions to IS *vs* concentration of each analyte on MS Excel 2016 (Fig. 5). Linear correlation between two variables was assessed by calculating the correlation coefficient. Equations of the calibration curves were used to quantify the unknown concentration of respective compounds present in the total extract.

2.13. Homology modelling

All sequence data were obtained from Uniprot. The accession numbers for baker's yeast α-glucosidase and isomaltase are P53341 and P53051, respectively. Sequence alignment of target and template was performed with ClustalW (Thompson et al., 1994) using BLOSUM62 matrix, gap opening penalty 10 and gap extension penalty 0.2 values. Homology modelling was performed through the web-based port of the Automated Comparative Protein Modelling Server (SWISSMODEL) (Waterhouse et al., 2018). The resulting homology structure was assessed using the protein structure verification tools PROCHECK (Laskowski et al., 1993), Verify3D (Luthy et al., 1992), PROVE (Pontius et al., 1996), ERRAT (Colovos and Yaetes, 1993) and WHATCHECK (Hooft et al., 1996). The model was visualised on Discovery Studio 2.5.5.

2.14. Docking settings

Docking experiments were conducted employing LigandFit docking engine within Discovery Studio 2.5.5 suite. LigandFit considers the flexibility of the ligand and recognises the receptor to be rigid. In the current docking experiments, the binding site was generated from the co-crystallized ligand of α-amylase applying "Find sites as volume of selected ligands" in Discovery Studio 2.5.5. While "Find sites from receptor cavities" tool was applied to find the binding site of α-glucosidase homology model. The following docking configurations were applied; energy grid: CFF force field with a nonbonded cutoff distance = 10.0 Å and distance-dependant dielectric and an energy grid extending 3.0 Å from the binding site using soft potential energy approximations; number of Monte Carlo trials = 30,000; the RMS threshold for ligand/site match = 2.0 Å, employing a maximum of 1.0 binding-site partitions; rigid body ligand minimisation parameters = 40 steepest descent iterations followed by 80 BFGS-minimization iterations were applied to every orientation of the docked ligand. The best ten poses were further energy minimised within the binding site by implementing the "Smart Minimization" option for a maximum of 1000 iterations. High-ranking docked conformers/poses were scored using six scoring functions: Jain, LigScore1, LigScore2, PLP1, PLP2, and PMF.

2.15. Statistical analysis

All the experiments were performed in triplicates, and final values were expressed as mean ±SD (standard deviation). The IC_{50} values were calculated using Graphpad Prism 6.04 (La Jolla, Califonia, USA). Microsoft Excel® was used in the calculation of the linear regression and the R^2 values. All the results produced in triplicates were further analysed by SPSS 25.0 to perform Analysis of Variance (ANOVA). Analysis of triplicate mean values was employed by Turkey`s post-test. P values < 0.05 were considered as statistically significant.

3. Results and discussion

3.1. LC-HRMS dereplication analysis

Dereplication analysis of LC-HRMS data of defatted MeEx of leaves and twigs of *S. grandiflora* revealed a total of 32 hits (Table 1). As indicated in Table 1, the MeOH extract of *S. grandiflora* is rich in flavonoids, flavonoid glycosides and terpenoids. During the literature survey, known compounds were reported with associated activities that demonstrate the scientific rationale of different biological activities (Mustafa et al., 2010; Baessa et al., 2019). For example, most of the flavonoid glycosides have been reported with potent antioxidant, anti-

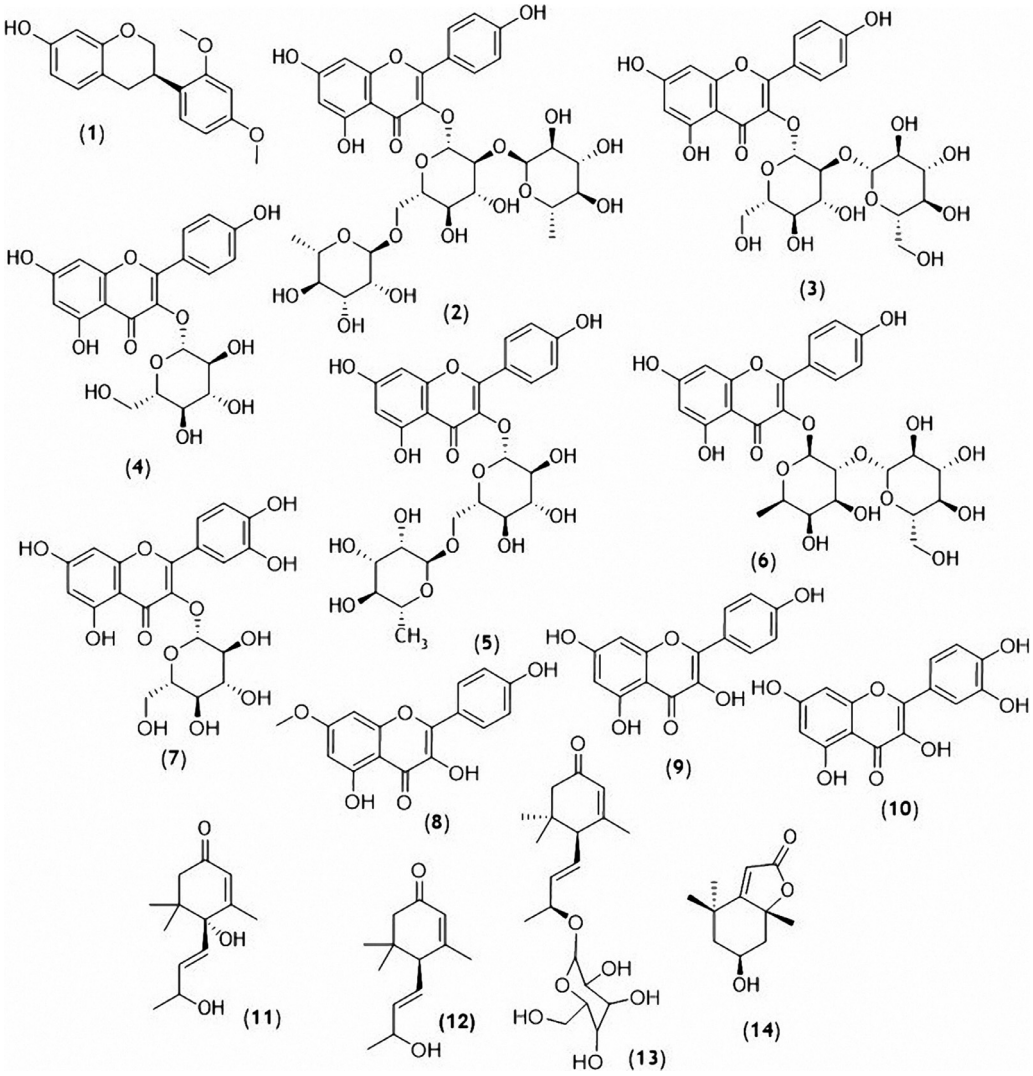

Fig. 1. Structures of isolated compounds **1**–**14**.

inflammatory and anti-diabetic properties while some flavonoids such as kaempferol and quercetin also showed potential antioxidant and antidiabetic activities under different *in vitro* screening methods (Vinayagam et al., 2015; Sarian et al., 2017). Moreover, dereplicated compounds with potent anti-tumour activities were identified, such as rhamnocitrin and chrysin dimethyl ether. Several terpenes such as different types of megastigmane derivatives as well as mono and diterpenes which have not been studied extensively for biological importance were also identified. The diverse chemical profile of *S. grandiflora* which was recorded for the first-time using LC-HRMS dereplication encouraged us to isolate and identify the major secondary metabolites present and evaluate their biological activities.

3.2. Phytochemistry

Column chromatographic separation followed by HPLC purification of the methanolic extract of *S. grandiflora* led to isolation of 14 known compounds (Fig. 1) including four flavonoids: sativan (**1**) (Shakeel et al., 2016), rhamnocitrin (**8**) (Baek et al., 2019), kaempferol (**9**) (Napolitano et al., 2012) and quercetin (**10**) (Feng-zhi et al., 2005); six flavonoid glycosides: kaempferol-3−2G-rhamnosylrutinoside (**2**) (Kazuma et al., 2003), panasenoside (**3**) (Liu et al., 2009), kaempferol-3-O-β-D-galactoside (**4**) (Wei et al., 2011), kaempferol-3-O-(6″-α-rhamnopyranosyl)-β-glucopyranoside (**5**) (Sang et al., 2001), kaempferol-3-O-β-D-glucopyranosyl(1−2)-α-L-rhamnoside (**6**) (Zhou et al., 2014) and isoquercitrin (**7**) (Mezache et al., 2010): three terpenoids; vomifoliol (**11**) (Metuno et al., 2008), megastigmane-3-oxo-α-ionol (**12**) (Pabst et al., 1992), loliolide (**14**) (Cho et al., 2016) and, one derivative of megastigmane glycoside: 3-oxo-α-ionol β-D-glucoside (**13**) (Pabst et al., 1992) were isolated for the first time from *S. grandiflora*. All the compounds isolated were fully characterised by 1D and 2D NMR and LC—HRESIMS data referring to literature and complied with dereplication results (Table 1). However, due to the polar nature and close structural similarity of these compounds (Fig. 2), we were not able to purify the rest of them, specifically megastigmane derivatives and some flavonoid glycosides and indeed some of them were isolated as non-separable mixtures.

3.3. α-Amylase and α-glucosidase inhibitory activity

The α-amylase inhibitory pattern (IC_{50} values) of the compounds is presented in Fig. 3. IC_{50} value depicts the amount of compound required to inhibit the enzyme activity by 50%. Thus, lower the IC_{50} value higher is the inhibitory activity. According to the results, the IC_{50} value of the compounds ranged between 17.45 to 2093 μM where compound **10** showed the highest activity (17.45 μM) followed by compound **9** (28.48 μM) while the least activity was observed in compound **1, 8**, and **11**. The IC_{50} value (8.4 μM) of the positive control acarbose was significantly higher than compounds **1, 8** and **11** (p <0.05). Compared to acarbose, compounds **9** and **10** (p <0.05) showed a potent α-amylase inhibitory activity where the activities were around 3.5 and 2 fold lower than acarbose, respectively. The inhibition pattern of the total MeEx and fraction Fr_3

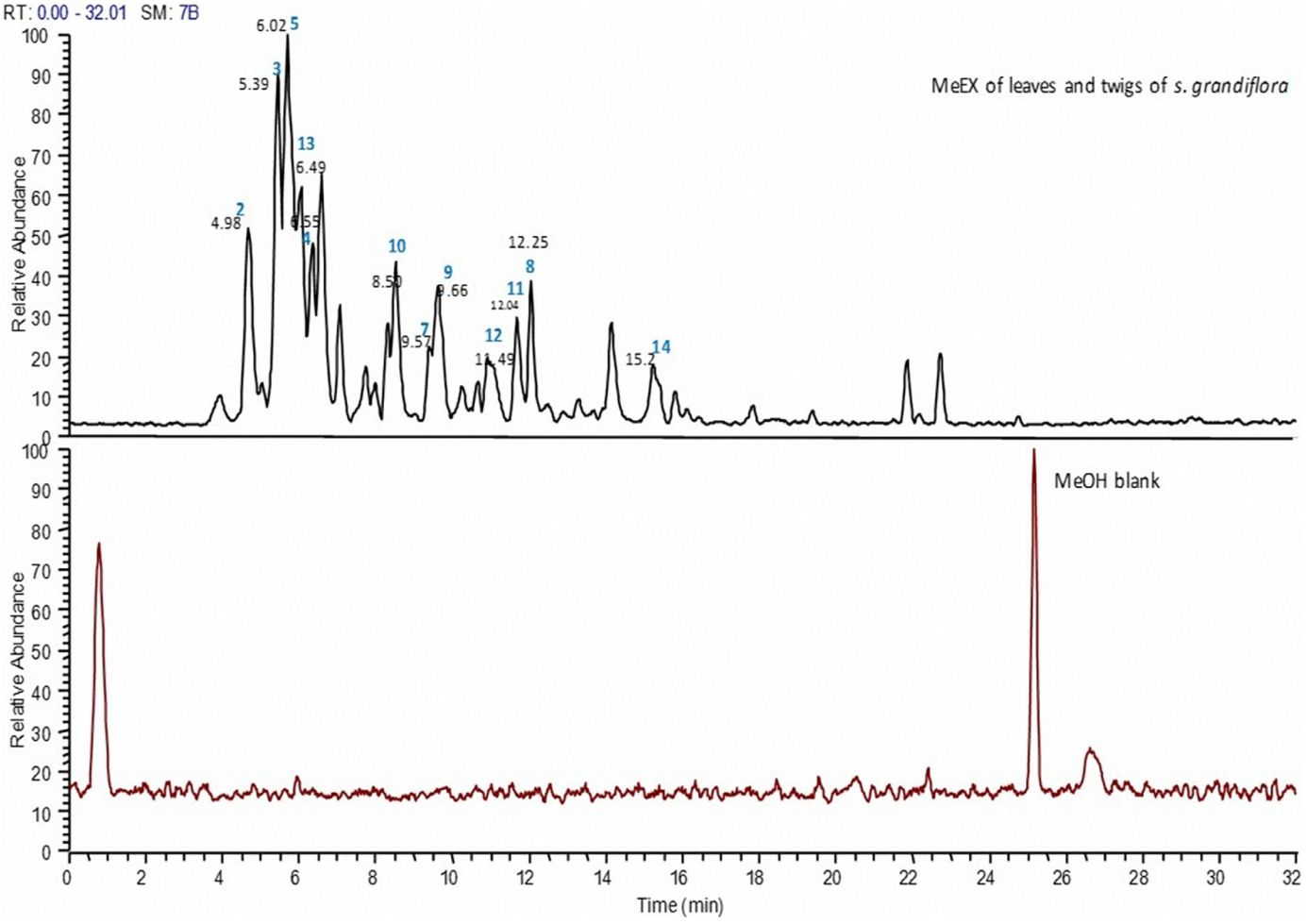

Fig. 2. Positive mode base peak chromatogram of MeEx of *S. grandiflora* to indicate most of the isolated compounds identified during dereplication.

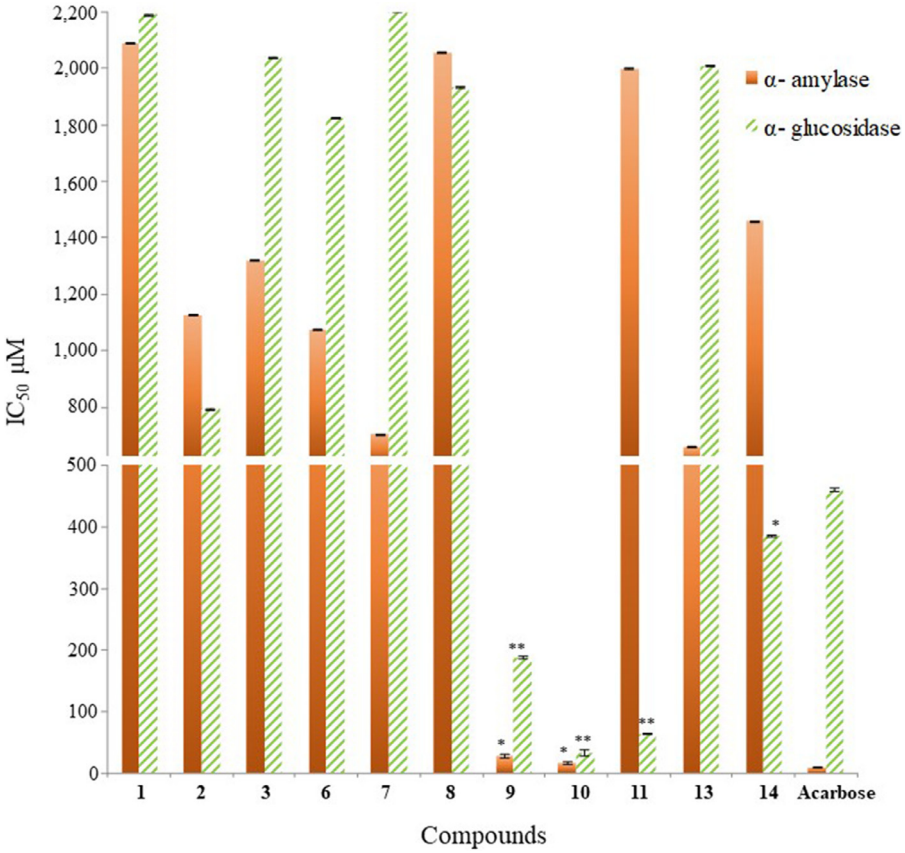

Fig. 3. α-Amylase and α-glucosidase inhibitory activity of the isolated compounds. * $p < 0.05$- Compound *vs* Acarbose, ** $p < 0.01$ Compound *vs* Acarbose.

showed with IC_{50} values >100 μg/mL and activities were statistically non-significant ($p > 0.05$), while it was 42 μg/mL for Fr_1 with a higher statistical difference ($p < 0.05$) compared to the total MeEx and Fr_3. Inhibition values of Fr_3 and Fr_1 further explained the activities exhibited by individual compounds isolated from these fractions.

The α-glucosidase inhibitory activity of the tested compounds ranged between 34.39 and 4864 μM (Fig. 3). The compounds showed a similar inhibitory pattern as α-amylase where compound **10** showed the highest activity against α-glucosidase followed by compound **9**. The least activity was recorded in compound **7**. Interestingly, compound **9, 10,** and **11** showed far better activities than the positive control acarbose (IC_{50} 484 μM) ($p < 0.01$) while compound **11** has also been much more efficient ($p < 0.05$). According to the results, the activity of compound **10** was found to be 14 times higher than that of acarbose, whereas compounds **9, 11**, and **14** had activities of 2.5, 7.5 and 1.2 times higher than acarbose, respectively. Activities of compounds **9** and **10** are in good agreement with the previously reported activities even with different methodology followed (Escandón-Rivera et al., 2012). Compound **12**, which is structurally similar to compound **11,** showed only 12% inhibition at 1 mM; thus its IC_{50} was not calculated. The activity discrimination between these two compounds was clearly demonstrated during docking studies highlighting the importance of OH group in the 6th position of compound **11** to inhibit the action of α- glucosidase. The isolated quantities of compound **4** and **5** were not enough to achieve the required assay concentrations, so they were not included in the assay. The inhibition pattern of the total MeEx, Fr_1 and Fr_3 correlated well with the activities depicted by their individual compounds. The IC_{50} values 92, 36 and 64 μg/mL (p <0.05) for the total MeEx, fraction Fr_1 and Fr_3 respectively, showed potent inhibition against α-glucosidase.

Postprandial hyperglycaemia is a major contributor to the development of DM. Thus, having good control on the blood glucose level is considered as one of the main strategies in the prevention of diabetes and associated complications (Castro-Acosta et al., 2017; Rasouli et al., 2017). Carbohydrases present in the gut, mainly α-glucosidase and α-amylase, play a significant role in the rise of blood glucose level after a meal (Rasouli et al., 2017; Pyner et al., 2017). Starch digestion begins in the oral cavity where it is first digested by the salivary α-amylases. The partially digested carbohydrates enter the intestine where they are further digested by the pancreatic α-amylases and the intestinal brush border α-glucosidases (Whitcomb and Lowe, 2007). There are different applied strategies for the treatment of DM among which the inhibition of starch hydrolysing enzymes; mainly amylase and glucosidase, are considered as a good strategy in the treatment of DM (Rasouli et al., 2017). Inhibition of these enzymes can aid in retarding carbohydrate digestion, thereby reducing the rate of glucose release into the bloodstream. According to the results, some of the tested compounds were found to show promising inhibitory activity against α-amylase and α-glucosidase. Especially, compound **9, 10** and **11** showed greater potent inhibitory activity against α-glucosidase than the drug acarbose, which is a well-known inhibitor of α-amylase and α-glucosidase to treat hyperglycaemia (Robyt, 2005; Villa-Rodriguez et al., 2017). α-Glucosidase, mainly found in the intestinal brush border, has a function to hydrolyse polysaccharides to its respective monomer (Poongunran et al., 2015; Xiao et al., 2006). α-Amylase secreted by the pancreas and salivary glands is mainly involved in hydrolysing starches into maltose and maltotriose (Visvanathan et al., 2016, 2019). Since our intestinal cells are only capable of absorbing monosaccharides, inhibition of α-glucosidases can be considered more crucial than inhibition of α-amylase to impede the uncontrollable rise in blood glucose level after a meal.

Table 2
Antioxidant capacity of the isolated compounds.

Compound	ABTS radical scavenging activity (mM TE/g) ± SD
1	4794±51
2	3882±60
3	6476±82
4	NT
5	NT
6	3477±35
7	4040±80
8	3377±66
9	40881±266***
10	99086±410***
11	15795±72**
12	4858±24
13	20261±66
14	13105±171**
Total MeEx	72896±185

Values are presented as mean standard deviation (± SD). NT- Not tested (insufficient quantity).
** $p < 0.001$.
*** $p < 0.01$.

3.4. ABTS radical scavenging activity

The tested compounds showed potent antioxidant activity in scavenging the ABTS radicals over 6 min. The activity of the compounds ranged between 3377±66 to 99086±410 mM TE/g (Table 2). Compound **10** displayed the highest total antioxidant activity, followed by compound **9** compared to all the other tested compounds ($p < 0.001$). Compound **11** and **14** also showed comparatively higher antioxidant activity ($p < 0.01$). They were also found to show promising anti-diabetic activity in terms of α-amylase and α-glucosidase inhibitory activities. The least radical scavenging activity was observed in compound **8, 6** and **2** which was non-significant ($p > 0.05$). Compound **4** and **5** were not included as their quantities were insufficient for full analysis.

3.5. Quantification of potent enzyme inhibitors

Quantification of quercetin, kaempferol, vomifoliol and loliolide which were identified with potential antidiabetic properties were quantified using HPLC. The chromatographic method was developed following EMA (European Medical Agency) guidelines, ICH guidelines and associated literature. Four calibration curves for the compounds **9, 10, 11** and **14** have shown a good linearity with correlation coefficients (R^2= 0.998–0.993). In the reported literature for quantitative analysis of terpenes, the ideal method of quantification was suggested as GC-MS for the small terpenes and LC-MS for the larger ones with more than 15 carbons in the carbon skeleton (Jiang et al., 2016). Both vomifoliol and loliolide in this study are small terpenes which were purified under semi-preparative HPLC conditions. The quantities of pure compounds left in our hands and the complex nature of the total MeEx of *S. grandiflora* discouraged us from using the GC-MS for the quantification of vomifoliol and loliolide using terpene specific IS. Nonetheless, we were able to carry out this quantitative analysis using HPLC as we have gained the knowledge of their characteristics and behaviour on HPLC during the purification. Different attempts to develop and optimise a chromatogram with a good peak resolution for the complex MeEx of *S. grandiflora* using different columns, solvent systems and parameters were applied. However, due to the close structural and chemical similarities between compound **9** and **10**, a complete separation of two peaks was not achieved under all the parameters applied during method optimisation and instead, a non-significant overlap was observed (Fig. 4). Quantitative analysis has revealed the most abundant active lead as quercetin (73.6 mg) followed by kaempferol (45.5 mg), vomifoliol (26.0 mg) and loliolide (12.3 mg) per 1 g of dry leaves of *S. grandiflora*. The quantitative analysis of these four enzyme inhibitors leads in the plant total extract well explained the biological activity of the *S. grandiflora*.

3.6. Docking experiments and homology modelling of α-glucosidase

To gain better insight into the ligand–enzyme binding interactions, it was decided to dock active compounds inside the substrate-binding site of α-amylase and α-glucosidase. Such experiments are very crucial to understand the SAR and to explain the biological variations among tested compounds. Molecular docking was conducted employing LigandFit docking engine. The resulting docking poses were scored by six different scoring functions: Jain, LigScore1, LigScore2, PLP1, PLP2, and PMF. The best-docked pose was

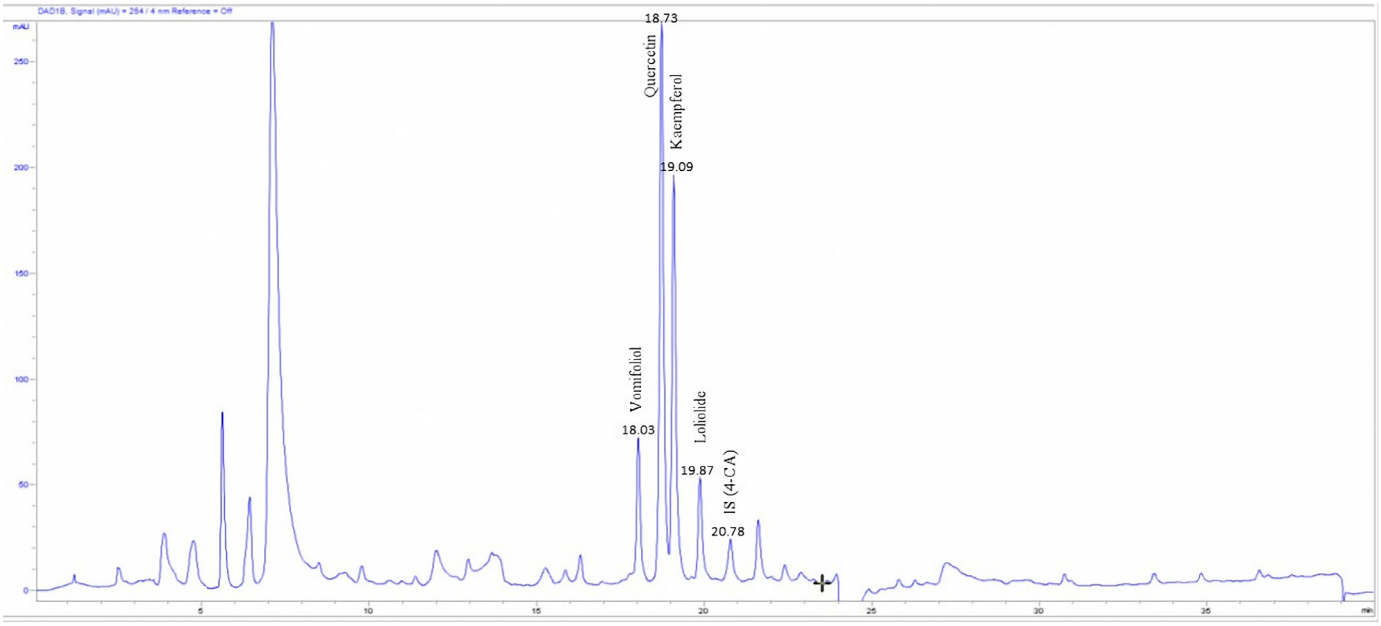

Fig. 4. HPLC chromatogram of the total MeEx of *S. grandiflora*.

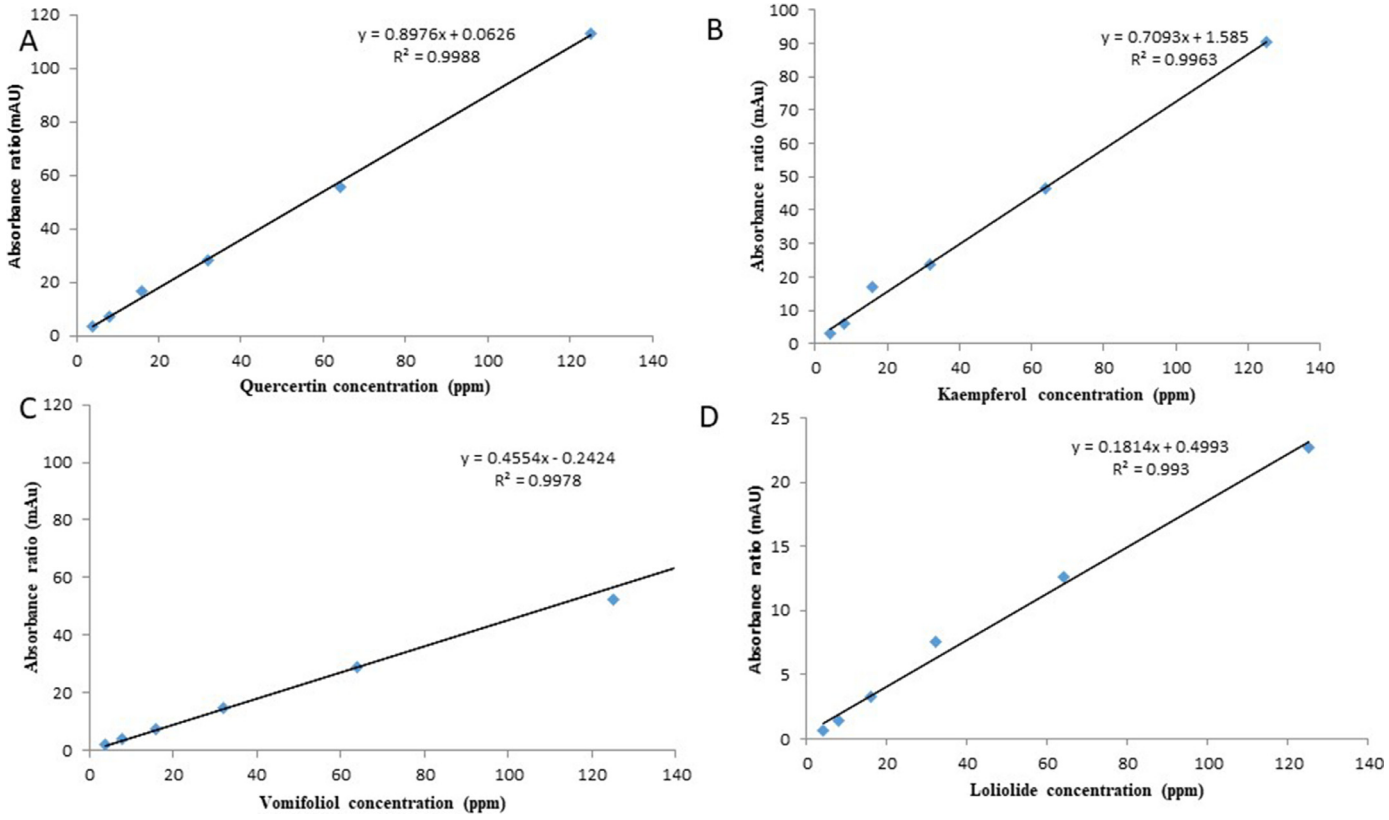

Fig. 5. Calibration curves of the anti-diabetic compounds; A. Quercetin B. Kaempferol C. Vomifoliol D. Loliolide.

selected based on consensus among all 6 scoring functions (Khanfar et al., 2013).

The 3D structure of pancreatic α-amylase was retrieved from protein data bank (PDB), and the X-ray crystallographic structure code (4GQR) was selected based on high structural similarity of the co-crystallized ligand to our compounds and based on its high resolution (1.2 Å) (Williams et al., 2012). Fig. 6 shows the docked pose of quercetin (**10**, IC_{50} α-amylase = 17.45 μM) into the putative binding pocket of α-amylase. The benzopyrone ring forms three hydrogen-bonding interactions with GLN63 and THR163. Alternatively, the catechol ring is π-stacked with phenolic ring of TYR62, while the catechol hydroxylic groups are chelated with carboxylate moiety of ASP197 through electrostatically enforced hydrogen bonding interactions. These interactions can explain the high inhibitory activity of quercetin against α-amylase, and subsequent loss of any interaction will significantly decrease the binding affinity toward α-amylase. For example, kaempferol (**9,** IC_{50} = 28.48 μM) shares all of the quercetin interactions except one; the chelation with ASP197, which could explain more than 50% loss of inhibitory activity as compared to quercetin (Fig. 7A & B). Moreover, rhamnocitrin (**8**), the 7-methoxy derivative of kaempferol (**9**), is almost an inactive compound. This can be attributed to methylation of 7-OH benzopyrone ring that used

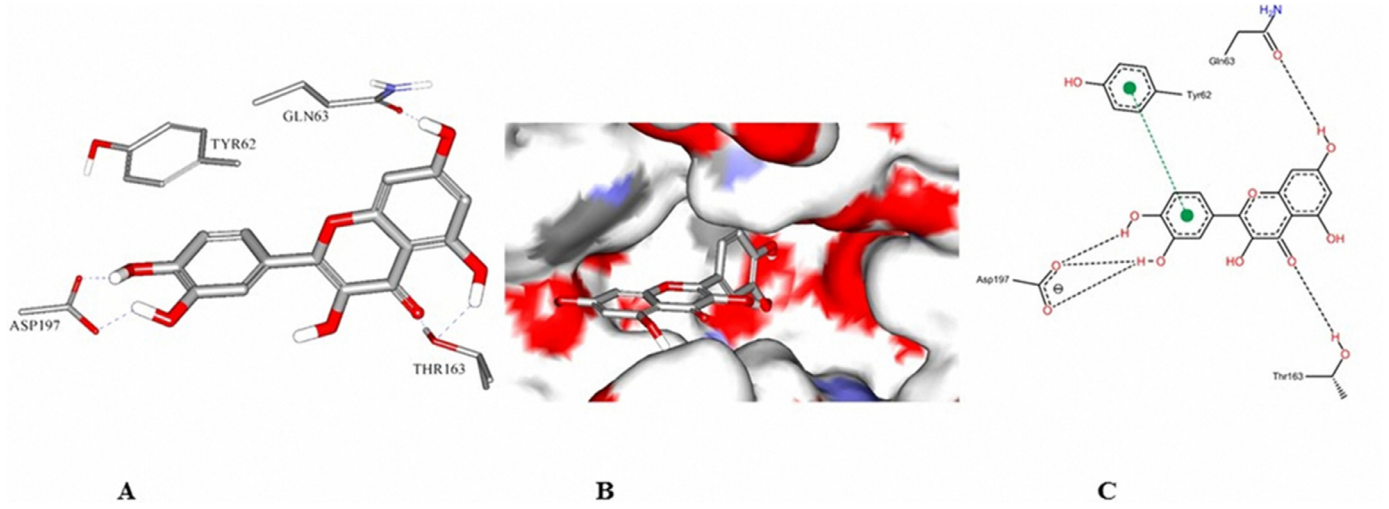

Fig. 6. (A) Highest-ranking docked pose of quercetin (**10**) into α-amylase (PDB code 4GQR) binding site. Hydrogen bonds are shown as blue dotted lines. (B) Connolly's surface of α-amylase binding site docked with quercetin (**10**). (C) 2D binding interaction diagram of quercetin (**10**) as generated by PoseView tool from ProteinsPlus web portal.

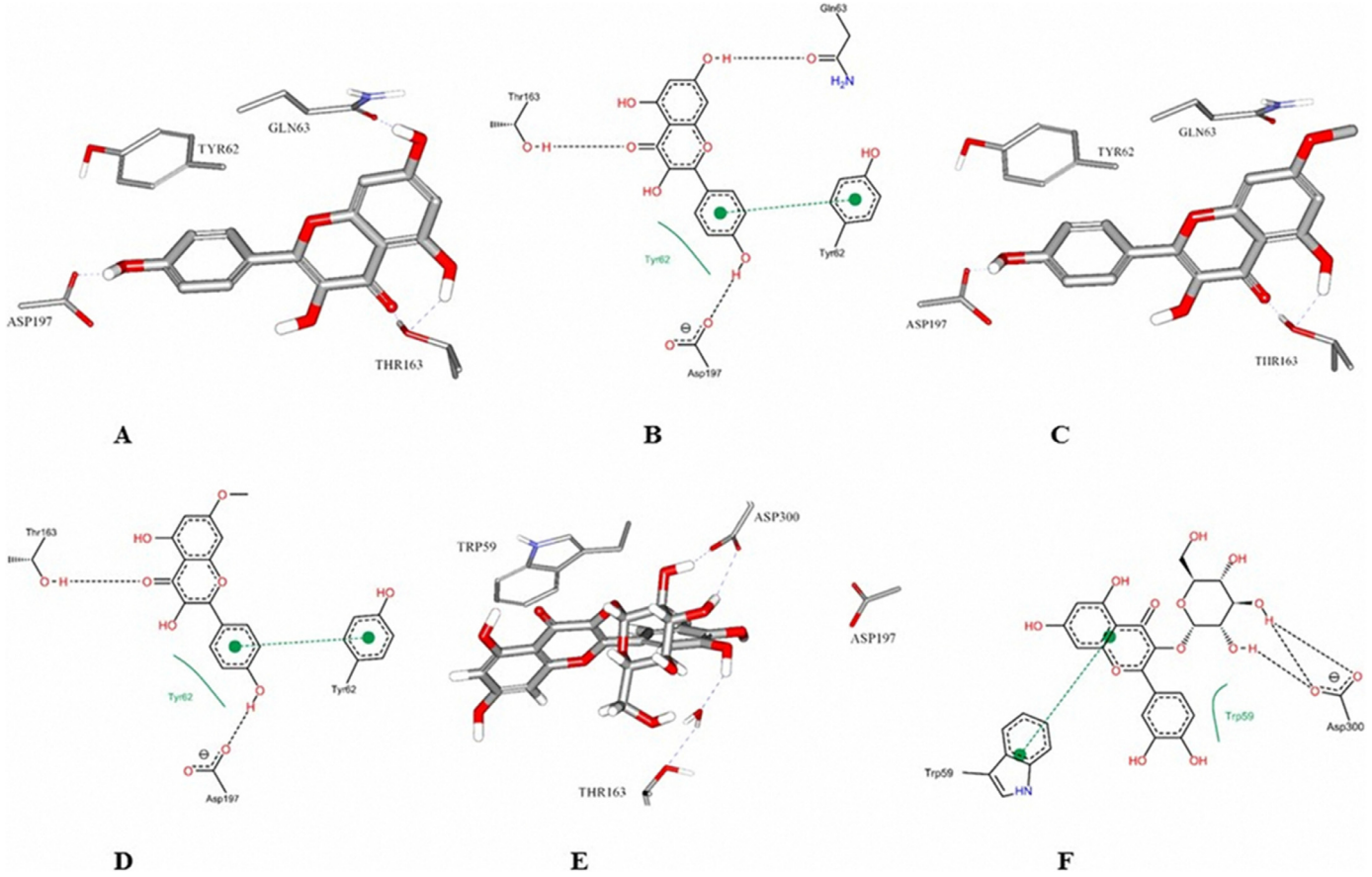

Fig. 7. (A), (C), and (E) are the highest-ranking docked poses of kaempferol (**9**), rhamnocitrin (**8**), and isoquercitrin (**7**), respectively, into α-amylase binding site (PDB code 4GQR). Hydrogen bonds are shown as blue dotted lines. (B), (D), (F) are the 2D binding interaction diagrams of kaempferol (**9**), rhamnocitrin (**8**), and isoquercitrin (**7**), respectively, as generated by PoseView tool from ProteinsPlus web portal.

to act as hydrogen−bond donor with GLN63, which highlights the significance of free benzopyrone hydroxylic groups for binding into the α-amylase active site (Fig. 7C & D).

On the other hand, docking was performed to understand the significant drop in α-amylase inhibitory activity upon glycosidation of quercetin [*e.g.*, isoquercitrin (**7,** IC_{50} = 704.84 μM), with about 40-fold decrease in IC_{50} value]. Docking studies of isoquercitrin (**7**) showed that this compound lost most of the interactions seen with quercetin, specifically the chelation with ASP197 and hydrogen-bonding interaction with GLN63 (Fig. 7E & F). Isoquercitrin is a highly branched compound that hinders its ability to access into the highly impeded hot-spots ASP197 and GLN63. Alternatively, the sugar moiety is hydrogen-bonded with the more reachable ASP300, while the catechol hydroxyl is water-bridged with THR163. Moreover, the

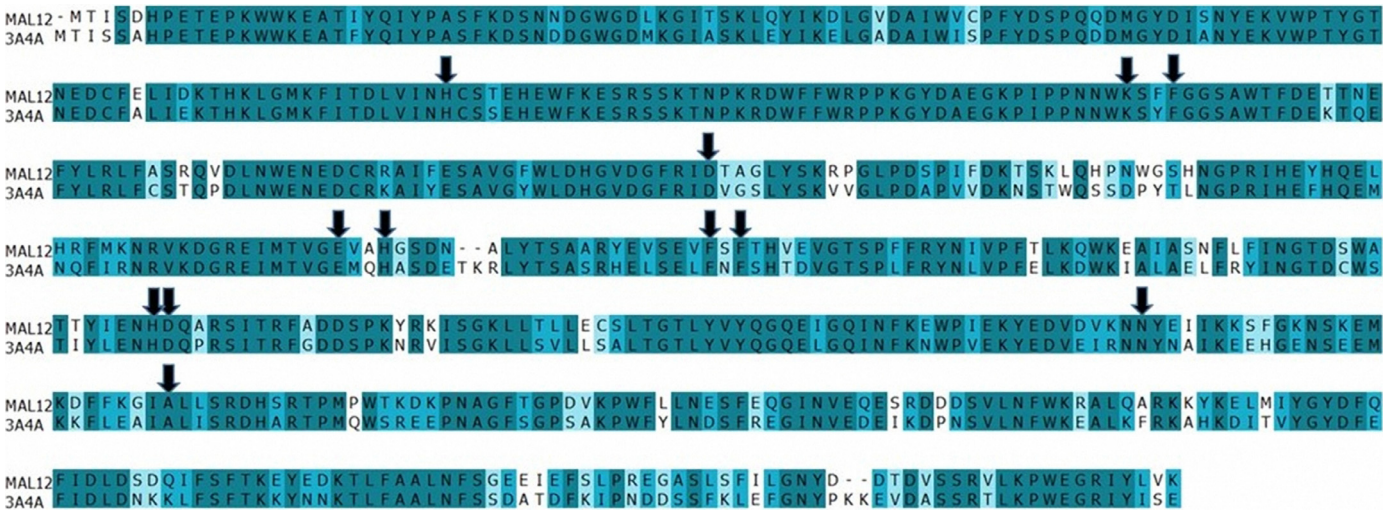

Fig. 8. Sequence alignment of α-glucosidase (MAL12_YEAST) and isomaltase (MALX3_YEAST, PDB code 3A4A). Both enzymes share 72% identity and 84% similarity. Identical catalytic binding site amino acids are marked by black arrows.

highest-ranked docked pose of isoquercitrin has significant desolvation penalty; only three out of eight hydroxylic groups could form hydrogen-bonding interactions, which might additionally explain the significant loss in α-amylase inhibitory activity.

The crystallographic structure of α-glucosidase of *Saccharomyces cerevisiae* (baker's yeast) has not been resolved yet; therefore, we were prompted to build a homology model of this protein. Sequence analysis of α-glucosidase showed that the optimum template for homology modelling is isomaltase from the same organism (EC 3.2.1.10, MALX3, PDB code 3A4A, Resolution: 1.6 Å, which shares 71% identity and 84% similarity with α-glucosidase). Homology modelling was performed employing SWISS-MODEL server (Waterhouse et al., 2018) and based on ClustalW (Thompson et al., 1994) pair-wise alignment. Sequence analysis showed high sequence homology with the target enzyme with 72% sequence identity alignment (Fig. 8). Interestingly, the binding site amino acids in the homology model of α-glucosidase are identical with their counterparts in isomaltase template, which enhances confidence in the accuracy of the homologous binding site (Fig. 8). The final structure of α-glucosidase was evaluated using PROCHECK (Laskowski et al., 1993), Verify3D (Luthy et al., 1992), PROVE (Pontius et al., 1996), ERRAT (Colovos and Yeates., 1993), and WHATCHECK (Hooft et al., 1996) protein check tools. The results of structure validation and quality are summarized in Table 3, which demonstrate excellent overall quality of α-glucosidase homology model. The Ramachandran plot obtained from PROCHECK showed that 89.1% of residues of the final 3D structure lied in most favoured regions (Fig. 9).

With the availability of plausible structure of α-glucosidase, we proceeded to docking experiment. The most active flavonoid inhibitor (quercetin **10**, IC_{50} α-glucosidase = 34.39 μM) showed strong binding interactions within the substrate binding site. The benzopyrone ring is hydrogen bonded with ASN241 and GLU304, while the catechol hydroxylic groups are chelated with ASP408 and hydrogen bonded to ASN412 along with a hydrophobic interaction of the same ring with PHE157 (Fig. 10). The observed hydrogen-bonding interactions are crucial for binding affinity to α-glucosidase. For example, removal of *meta*-OH catecholic group (as in kaempferol (**9**), IC_{50} α-glucosidase = 188.89 μM) resulted in 5.5- fold decrease in activity. This can be clearly explained by missing two interactions with ASP408 and ASN412 (Fig. 11A & B). Nevertheless, additional methylation of 7-OH benzopyrone moiety resulted in a weak α-glucosidase ligand (rhamnocitrin **8**). The former drop in activity is attributed to the interruption of electrostatically enforced hydrogen bonding interaction with carboxylate moiety of ASP304.

Moreover, docking was conducted to understand the binding affinity of active terpenoids. Fig. 11C and D showed how vomifoliol (**11**, IC_{50} α-glucosidase = 64.4 μM) binds within α-glucosidase binding site. The enone carbonyl oxygen is hydrogen bonded to ASN241,

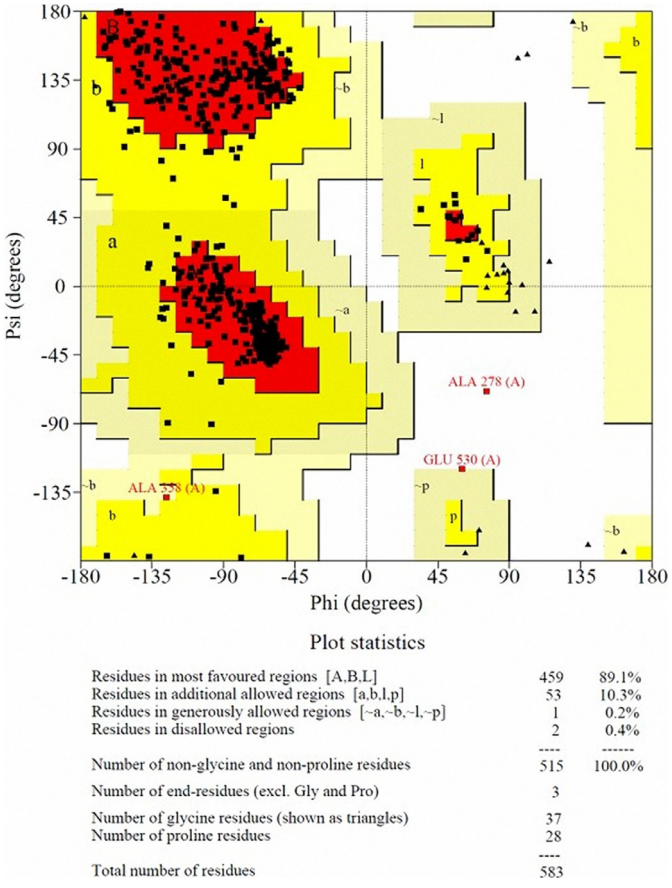

Fig. 9. Ramachandran plot of α-glucosidase homologue model based on isomaltase template (PDB code 3A4A).

while the 6-OH is forming two hydrogen-bonding interactions with HIS279 and GLU304. The former interactions seem to be very critical, as the 6-deoxy analogue (megastigmane-3-oxo-α-ionol **12**) is an inactive compound. The other terpenoid compound that was found to be moderately active is loliolide (**14**, IC_{50} α-glucosidase = 399.36 μM). The binding of this compound is mostly hydrophobic against two hydrophobic surfaces of PHE157 and PHE300 side chains (Fig. 11E & F). Alternatively, the lactone carbonyl oxygen and 6-hydroxy groups are hydrogen bonded with ASN241 and GLU304, respectively.

The highly branched flavonoid glycosides along with their high desolvation penalties can explain their poor binding affinities against α-glucosidase. Fig. 10B shows how narrow is the gate of α-glucosidase binding site hindering the entry of such branched compounds.

Table 3
The results of structure validation of α-glucosidase homologue model as tested by PROCHECK, Verify3D, PROVE, ERRAT, and WHATCHECK protein check tools.

PROCHECK[a]	Verify3D[b]	PROVE[c]	ERRAT[d]	WHATCHECK							
89.1%	95.36%	3.2%	96.7%	Overall summary report: Pass							
				1st generation packing quality[e]	Ramachandran plot appearance[e]	chi-1/chi-2 rotamer normality[e]	Backbone conformation[e]	Bond lengths[f]	Bond angles[f]	Omega angle restraints[f]	Side chain planarity[f]
				−0.730	−0.729	−0.046	−1.422	0.691	1.087	1.264	1.334

[a] 89.1% of residues of the final 3D structure lied in most favoured regions.
[b] 95.36% of the residues have averaged 3D-1D score ≥ 0.2.
[c] % buried atoms: > 5% ERROR, 1% to 5% Warning, < 1% Pass.
[d] Overall quality factor, expressed as the percentage of the protein for which the calculated error value falls below the 95% rejection limit. Good high-resolution structures generally produce values around 95% or higher.
[e] Structure Z-scores, positive is better than average.
[f] RMS Z-scores, closer to 1.0 is better.

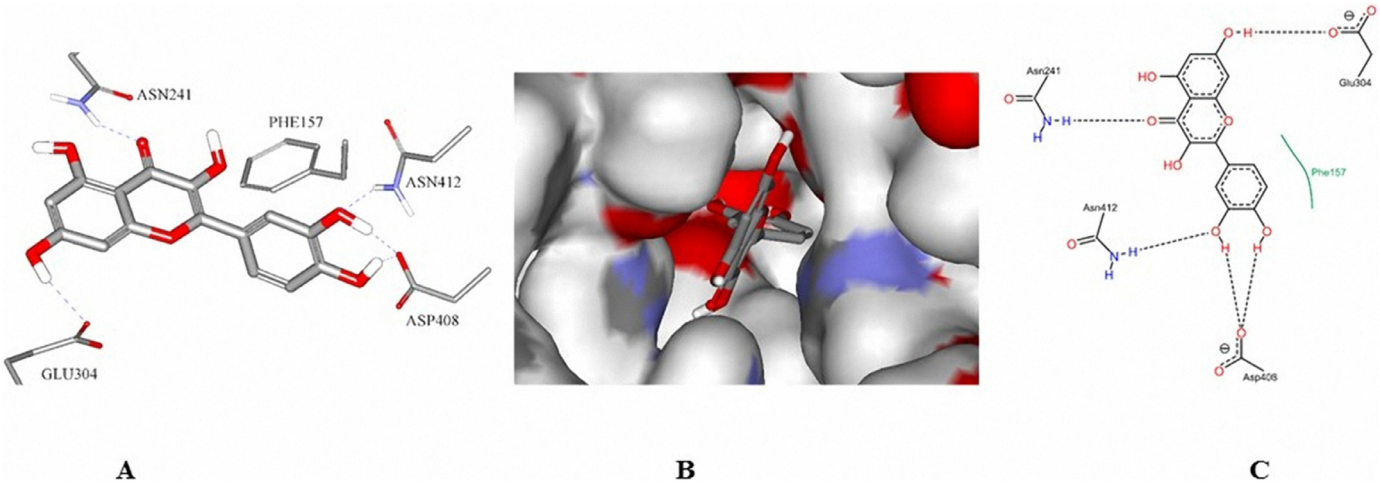

Fig. 10. (A) Highest-ranking docked pose of quercetin (**10**) into the homology model of α-glucosidase binding site. Hydrogen bonds are shown as blue dotted lines. (B) Connolly's surface of α- glucosidase binding site docked with quercetin (**10**). 2D binding interaction diagram of quercetin (**10**) as generated by PoseView tool from ProteinsPlus web portal.

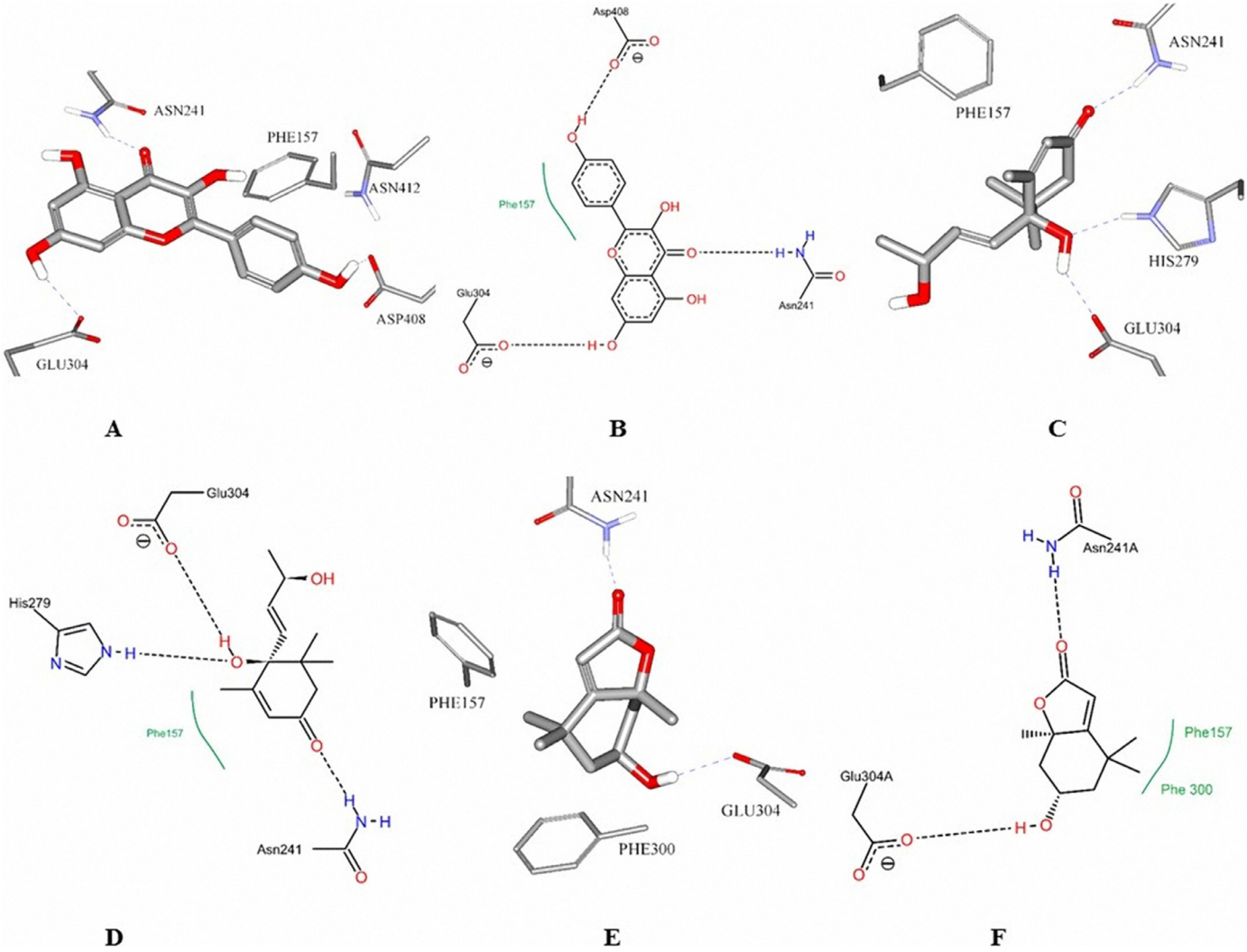

Fig. 11. (A), (C), and (E) are the highest-ranking docked poses of kaempferol (**9**), vomifoliol (**11**), and loliolide (**14**), respectively, into the homology model of α-glucosidase binding site. Hydrogen bonds are shown as blue dotted lines. (B), (D), (F) are the 2D binding interaction diagrams of kaempferol (**9**), vomifoliol (**11**), and loliolide (**14**), respectively, as generated by PoseView tool from ProteinsPlus web portal.

4. Conclusion

In summary, we report, for the first time the chemical profile of *S. grandiflora*, which is a well-known edible medicinal plant growing in Sri Lanka, with 32 possible phytochemical hits by using LC-HRMS dereplication profiling. Bio-guided fractionation of *S. grandiflora* crude extract led to the isolation of 14 known compounds belonging to flavonoid and terpenoid classes for the first time from this plant species. Although the total extract was proved to have moderate *in vitro* antidiabetic activity when screened against streptozotocin-induced diabetic rat/mice, strong *in vitro* inhibitory effects against α-amylase and α-glucosidase, no chemical evidence or rationale was claimed in the literature. In the current study, four potent metabolites; quercetin, kaempferol, vomifoliol and loliolide were identified through *in vitro* screening as potential α-amylase and α-glucosidase inhibitors. Although the α-amylase and α-glucosidase inhibitory activities of quercetin, kaempferol were reported before, the inhibitory effect of the terpenoids vomifoliol and loliolide were discovered for the first time. This finding spots these two terpenoids as a new structural motif for the discovery of new antidiabetic scaffold. Additionally, all active compounds exhibited good radical scavenging properties making them more desirable to be developed as anti-diabetic agents. The inhibitory activities of all potent anti-diabetic agents have been further rationalised by molecular modelling, claiming that *S. grandiflora* is a promising dietary element to defence T2DM. Quantitative analysis of the most active molecules in the total *S. grandiflora* extract indicated their presence in reasonable quantities that could justify the folk use of the edible *S. grandiflora* for diabetic patients in Sri Lanka and other Asian countries. Furthermore, this will popularise the consumption of leaves of *S. grandiflora* as a potential remedy for controlling T2DM.

Declaration of Competing Interest

The authors declare that they have no known competing financial interests or personal relationships that could have appeared to influence the work reported in this paper.

Acknowledgements

We thank the College of Physical Sciences, University of Aberdeen, for the provision of infrastructure facilities in the Marine Biodiscovery Centre, and Prof. Marcel Jaspars, Marine Biodiscovery Centre for NMR and LC-HRMS analysis of our samples. We also thank Dr M.N. Napagoda, University of Ruhuna, Sri Lanka who authenticated the plant material.

Funding

This research did not receive any funding.

Supplementary materials

Supplementary material associated with this article can be found in the online version at doi:10.1016/j.sajb.2020.01.011.

References

Achenbach, H., Waibel, R., Addae-Mensah, I., 1985. Sesquiterpenes from *Carissa edulis*. Phytochemistry 24 (10), 2325–2328.

Adnan, M., Chy, N.U., Mostafa Kamal, A.T.M., Azad, M.O.K., Paul, A., Uddin, S.B., Barlow, J.W., Faruque, M.O., Park, C.H., Cho, D.H.,, 2019. Investigation of the Biological Activities and Characterization of Bioactive Constituents of Ophiorrhiza rugosa var. prostrata (D. Don) & Mondal Leaves through *In Vivo*, *In Vitro*, and *In Silico* Approaches. Molecules 24 (7), 1367. https://doi.org/10.3390/molecules24071367.

Al-Qudah, M.A., Otoom, N.K., Al-Jaber, H.I., Saleh, A.M., Abu Zarga, M.H., Afifi, F.U., et al., 2017. New flavonol glycoside from *Scabiosa prolifera* L. aerial parts with *in vitro* antioxidant and cytotoxic activities. Natural Products Research 31 (24), 2865–2874.

Anantaworasakul, P., Hamamoto, H., Sekimizu, K., Okonogi, S., 2017. Biological activities and antibacterial biomarker of *Sesbania grandiflora* bark extract. Drug Discovery Therapeutics 11 (2), 70–77.

Atanasov, A.G., Waltenberger, B., Pferschy-Wenzig, E.M., Linder, T., Wawrosch, C., Uhrin, P., et al., 2015. Discovery and resupply of pharmacologically active plant-derived natural products: a review. Biotech Advances 33 (8), 1582–1614.

Bae, S., D'cunha, R., Shao, J., An, G., 2018. Effect of 5, 7-dimethoxyflavone on BCRP1-mediated transport of sorafenib *in vitro* and *in vivo* in mice. European Journal of Pharmaceutical Sciences 117, 27–34.

Baek, S.C., Park, M.H., Ryu, H.W., Lee, J.P., Kang, M.G., Park, D., Park, C.M., et al., 2019. Rhamnocitrin isolated from *prunus padus* var. seoulensis: a potent and selective reversible inhibitor of human monoamine oxidase A. Bioorganic Chemistry 83, 317–325.

Baessa, M., Rodrigues, M.J., Pereira, C., Santos, T., da Rosa Neng, N., Nogueira, J.M.F., Ba., et al., 2019. A comparative study of the *in vitro* enzyme inhibitory and antioxidant activities of *Butea monosperma* (Lam.) Taub. and *Sesbania grandiflora* (L.) Poiret from Pakistan: new sources of natural products for public health problems. South Affrican Journal of Botany 120, 146–156.

Balasuriya, B.M.G.K., Dharmaratne, H.R.W., 2007. Cytotoxicity and antioxidant activity studies of green leafy vegetables consumed in Sri Lanka. Journal of National Science Foundation. Sri Lanka 35 (4).

Castro-Acosta, M.L., Stephanie, G.S., Jonathan, E.M., Rhia, K.M., Chi-leng Fu, G., 2017. Apple and blackcurrant polyphenol-rich drinks decrease postprandial glucose, insulin and incretin response to a high-carbohydrate meal in healthy men and women. Journal of Nutritional Biochemistry 49, 53–62.

Chen, G.L., Fan, M.X., Wu, J.L., Li, N., Guo, M.Q., 2019. Antioxidant and anti-inflammatory properties of flavonoids from *Lotus plumule*. Food Chemistry 277, 706–712.

Chen, Y.P., Tong, C., Lu, W.Q., Shen, Y.H., Wu, Z.J., Chen, W.S., 2019. Three new sesquiterpenes from Ainsliaea glabra. Natural Product Research 33 (2), 274–279.

Choudhary, M.I., Begum, A., Abbaskhan, A., 2006. Cinnamate derivatives of fructo-oligosaccharides from *Lindelofia stylosa*. Carbohydrate Research 341 (14), 2398–2405.

Cho, S., Lee, D.G., Jung, Y.S., Kim, H.B., Cho, E.J., Lee, S., 2016. Phytochemical identification from *Boehmeria nivea* leaves and analysis of (−)-loliolide by HPLC. Natural Product Sciences 22 (2), 134–139.

Colovos, C., Yeates, T.O., 1993. Verification of protein structures: patterns of nonbonded atomic interactions. Protein Science 2 (9), 1511–1519.

Das, J., Das, M.P., Velusamy, P., 2013. *Sesbania grandiflora* leaf extract mediated green synthesis of antibacterial silver nanoparticles against selected human pathogens. Spectrochimica Acta Part A: Molecular and Biomolecular Spectroscopy 104, 265–270.

Dong, H.Q., Li, M., Zhu, F., Liu, F.L., Huang, J.B., 2012. Inhibitory potential of trilobatin from *Lithocarpus polystachyus* REHD against α-glucosidase and α-amylase linked to type 2 diabetes. Food Chemistry 130 (2), 261–266.

Escandón-Rivera, S., González-Andrade, M., Bye, R., Linares, E., Navarrete, A., Mata, R., 2012. α-Glucosidase inhibitors from *Brickellia cavanillesii*. Journal of Natural Products 75 (5), 968–974.

Eom, H.J., Lee, D., Lee, S., Noh, H.J., Hyun, J.W., Yi, P.H., et al., 2016. Flavonoids and a limonoid from the fruits of *Citrus unshiu* and their biological activity. Journal of Agricultural Food Chemistry 64 (38), 7171–7178.

Feng-zhi, R.E.N., Gang-san, L.I.U., Zhang, L., Gui-yun, N.I.U., 2005. Studies on chemical constituents of Hedyotis diffusa willd. Journal of Chinese Pharmaceutical Sciences 40 (7), 502–504.

Frezza, C., De Vita, D., Spinaci, G., Sarandrea, M., Venditti, A., Bianco, A., 2018. Secondary metabolites of *Tilia tomentosa* Moench inflorescences collected in Central Italy: chemotaxonomy relevance and phytochemical rationale of traditional use. Natural Product Research 1–8.

Galasso, S., Pacifico, S., Kretschmer, N., Pan, S.P., Marciano, S., Piccolella, S., et al., 2014. Influence of seasonal variation on *Thymus longicaulis* C. Presl chemical composition and its antioxidant and anti-inflammatory properties. Phytochemistry 107, 80–90.

Goun, E., Cunningham, G., Chu, D., Nguyen, C., Miles, D., 2003. Antibacterial and antifungal activity of Indonesian ethnomedical plants. Fitoterapia 74 (6), 592–596.

Hussain, A.Z., Kumaresan, S., 2014. GC-MS studies and phytochemical screening of *Sesbania grandiflora* l. Journal of Chemical Pharmaceutical Research 6, 43–47.

Jiang, Z., Kempinski, C., Chappell, J., 2016. Extraction and analysis of terpenes/terpenoids. Current Protocols in Plant Biology 1 (2), 345–358.

Han, X.X., Jiang, Y.P., Liu, N., Wu, J., Yang, J.M., Li, Y.X., et al., 2019. Protective effects of astragalin on spermatogenesis in streptozotocin-induced diabetes in male mice by improving antioxidant activity and inhibiting inflammation. Biomedicine and Pharmacotherapy 110, 561–570.

Hao, J., Li, J., Li, X., Liu, Y., Ruan, J., Dong, Y., et al., 2016. Aromatic Constituents from the stems of *astragalus membranaceus* (Fisch.) BGE. var. Mongholicus (Bge.) Hsiao. Molecules 21 (3), 354.

Hasan, N., Osman, H., Mohamad, S., Chong, W.K., Awang, K., Zahariluddin, A.S.M., 2012. The chemical components of Sesbania grandiflora root and their antituberculosis activity. Pharmaceuticals 5 (8), 882–889.

Hooft, R.W., Vriend, G., Sander, C., Abola, E.E., 1996. Errors in protein structures. Nature 381 (6580), 272.

Johansen, J.S., Harris, A.K., Rychly, D.J., Ergul, A., 2005. Oxidative stress and the use of antioxidants in diabetes: linking basic science to clinical practice. Cardiovascular Diabetol 4 (5). https://doi.org/10.1186/1475-2840-4-5.

Kazuma, K., Noda, N., Suzuki, M., 2003. Malonylated flavonol glycosides from the petals of *Clitoria ternatea*. Phytochemistry 62 (2), 229–237.

Khanfar, M.A., AbuKhader, M.M., Alqtaishat, S., Taha, M.O., 2013. Pharmacophore modelling, homology modelling, and in silico screening reveal mammalian target of rapamycin inhibitory activities for sotalol, glyburide, metipranolol, sulfamethizole, glipizide, and pioglitazone. Journal of Molecular Graphics and Modelling 42, 39–49.

Kuo, Y.H., Chen, C.H., 1998. Sesquiterpenes from the leaves of *Tithonia diversifolia*. Journal of Natural Products 61 (6), 827–828.

Kwon, Y.I., Apostolidis, E., Shetty, K., 2008. Inhibitory potential of wine and tea against α-amylase and α-glucosidase for management of hyperglycemia linked to type 2 diabetes. Journal of Food Biochemistry 32 (1), 15–31.

Laladhas, K.P., Cheriyan, V.T., Puliappadamba, V.T., Bava, S.V., Unnithan, R.G., Vijayammal, P.L., et al., 2010. A novel protein fraction from *sesbania grandiflora* shows potential anticancer and chemopreventive efficacy, *in vitro* and *in vivo*. Journal of Cellular and Molecular Medicine 14 (3), 636–646.

Laskowski, R.A., MacArthur, M.W., Moss, D.S., Thornton, J.M., 1993. PROCHECK: a program to check the stereochemical quality of protein structures. Journal of Applied Crystallography 26 (2), 283–291.

Li, T., Kongstad, K.T., Staerk, D., 2019. Identification of α-glucosidase inhibitors in *machilus litseifolia* by combined use of high-resolution α-glucosidase inhibition profiling and hplc-pda-hrms-spe-nmr. Journal of Natural Products 82 (2), 249–258.

Lin, Y., Xu, W., Huang, M., Xu, W., Li, H., Ye, M., et al., 2015. Qualitative and quantitative analysis of phenolic acids, flavonoids and iridoid glycosides in *yinhua kanggan* tablet by uplc-qqq-ms/ms. Molecules 20 (7), 12209–12228.

Liu, F., Cao, W., Deng, C., Wu, Z., Zeng, G., Zhou, Y., 2016. Polyphenolic glycosides isolated from *pogostemon cablin* (Blanco) benth. as novel influenza neuraminidase inhibitors. Chemistry Central Journal 10 (1), 51.

Liu, C., Chen, J., Wang, J., 2009. A novel kaempferol triglycoside from flower buds of *Panax quinquefolium*. Chemistry of Natural Compounds 45 (6), 808–810.

Liyanage, R., Kiramage, C., Visvanathan, R., Jayathilake, C., Weththasinghe, P., Bangamuwage, R., et al., 2018. Hypolipidemic and hypoglycemic potential of raw, boiled, and sprouted mung beans (*Vigna radiata* L. Wilczek) in rats. Journal of Food Biochemistry 42 (1), e12457.

Luo, G., Ye, Q., Du, B., Wang, F., Zhang, G.L. and Luo, Y., 2016. Iridoid glucosides and diterpenoids from *caryopteris glutinosa*. Journal of Natural Products. 79(4), pp. 886−893.

Lüthy, R., Bowie, J.U., Eisenberg, D., 1992. Assessment of protein models with three-dimensional profiles. Nature 356 (6364), 83.

Lutz, A., Winterhalter, P., 1992. Abscisic alcohol glucoside in quince. Phytochemistry 32 (1), 57–60.

Macías, F.A., López, A., Varela, R.M., Torres, A., Molinillo, J.M., 2004. Bioactive apocarotenoids annuionones f and G: structural revision of annuionones A, b and e. Phytochemistry 65 (22), 3057–3063.

Macintyre, L., Zhang, T., Viegelmann, C., Martinez, I., Cheng, C., Dowdells, C., et al., 2014. Metabolomic tools for secondary metabolite discovery from marine microbial symbionts. Marine drugs 12 (6), 3416–3448.

Metuno, R., Ngandeu, F., Tchinda, A.T., Ngameni, B., Kapche, G.D., Djemgou, P.C., et al., 2008. Chemical constituents of *treculia acuminata* and *treculia africana* (Moraceae). Biochemical Systematics and Ecology 2 (36), 148–152.

Mezache, N., Bendjeddou, D., Satta, D., Mekkiou, R., Benayache, S., Benayache, F., 2010. Secondary metabolites from *Centaurea lippii*. Chemistry of Natural Compounds 46 (5), 801–802.

Milella, L., Milazzo, S., De Leo, M., Vera Saltos, M.B., Faraone, I., Tuccinardi, T., et al., 2016. α-Glucosidase and α-amylase inhibitors from *arcytophyllum thymifolium*. Journal of Natural Products 79 (8), 2104–2112.

Mustafa, R.A., Hamid, A.A., Mohamed, S., Bakar, F.A., 2010. Total phenolic compounds, flavonoids, and radical scavenging activity of 21 selected tropical plants. Journal of Food Science 75 (1), C28–C35.

Munde-Wagh, K.B., Wagh, V.D., Toshniwal, S.S., Sonawane, B.R., 2012. Phytochemical, antimicrobial evaluation and determination of total phenolic and flavonoid contents of *Sesbania grandiflora* flower extract. International Journal of Pharmaceutical Sciences 4 (4), 229–232.

Na Ranong, S., Likhitwitayawuid, K., Mekboonsonglarp, W., Sritularak, B, 2019. New dihydrophenanthrenes from Dendrobium infundibulum. Natural product research 33 (33), 420–426. https://doi.org/10.1080/14786419.2018.1455050.

Napolitano, J.G., Lankin, D.C., Chen, S.N., Pauli, G.F., 2012. Complete ^{1}H NMR spectral analysis of ten chemical markers of Ginkgo biloba. Magnetic Resonance in Chemistry 50 (8), 569–575.

Oboh, G., Ademiluyi, A.O., Akinyemi, A.J., Henle, T., Saliu, J.A., Schwarzenbolz, U., 2012. Inhibitory effect of polyphenol-rich extracts of jute leaf (*Corchorus olitorius*) on key enzyme linked to type 2 diabetes (α-amylase and α-glucosidase) and hypertension (angiotensin i converting) *in vitro*. Journal of Functional Foods 4 (2), 450–458.

Panigrahi, G., Panda, C., Patra, A., 2016. Extract of *sesbania grandiflora* ameliorates hyperglycemia in high fat diet-streptozotocin induced experimental diabetes mellitus. Scientifica. https://doi.org/10.1155/2016/4083568. Article ID 4083568.

Pabst, A., Barron, D., Sémon, E., Schreier, P., 1992. Two diastereomeric 3-oxo-α-ionol β-d-glucosides from raspberry fruit. Phytochemistry 31 (5), 1649–1652.

Park, J.H., Lee, D.G., Yeon, S.W., Kwon, H.S., Ko, J.H., Shin, D.J., et al., 2011. Isolation of megastigmane sesquiterpenes from the silkworm (*Bombyx mori* L.) droppings and their promotion activity on HO-1 and SIRT1. Archives of Pharmacal Research 34 (4), 533–542.

Pereira, M., Da Silva, T., Lopes, L., Krettli, A., Madureira, L., Zukerman-Schpector, J., 2012. 4, 5-seco-guaiane and a nine-membered sesquiterpene lactone from *holostylis reniformis*. Molecules 17 (12), 14046–14057.

Pontius, J., Richelle, J., Wodak, S.J., 1996. Deviations from standard atomic volumes as a quality measure for protein crystal structures. Journal of Molecular Biology 264 (1), 121–136.

Poongunran, J., Perera, H.K.I., Fernando, W.I.T., Jayasinghe, L., Sivakanesan, R., 2015. alpha-Glucosidase and alpha-amylase inhibitory activities of nine Sri Lankan antidiabetic plants. British Journal of Pharmacology 7 (5), 365–374.

Prasanna, G., Saraswathi, N., 2013. The therapeutic role of *sesbania grandiflora* as an inhibitor of advanced glycation endproduct (AGE) formation and the discovery of lead compounds for managing hyperglycaemia. Planta Medica 79 (13), 1268.

Pyner, A., Nyambe-Silavwe, H., Williamson, G., 2017. Inhibition of human and rat sucrase and maltase activities to assess antiglycemic potential: Optimization of the assay using acarbose and polyphenols. Journal of Agricultural Food Chemistry 65 (39), 8643–8651.

Qin, F.Y., Cheng, L.Z., Yan, Y.M., Liu, B.H., Cheng, Y.X., 2018. Choushenosides A-C, three dimeric catechin glucosides from *codonopsis pilosula* collected in yunnan province, china. Phytochemistry 153, 53–57.

Rasouli, H., Hosseini-Ghazvini, S.M.B., Adibi, H., Khodarahmi, R., 2017. Differential α-amylase/α-glucosidase inhibitory activities of plant-derived phenolic compounds: a virtual screening perspective for the treatment of obesity and diabetes. Food and Function 8 (5), 1942–1954.

Robyt, J.F., 2005. Inhibition, activation, and stabilization of α-amylase family enzymes. Biologia Bratislava 16, 17–26.

Roy, A., Bhoumik, D., Sahu, R.K., Dwivedi, J., 2014. Phytochemical screening and antioxidant activity of *Sesbania grandiflora* leaves extracts. Asian Journal of Pharmaceutical Sciences 4 (1), 16–21.

Ramesh, T., Mahesh, R., Sureka, C., Begum, V.H., 2008. Cardioprotective effects of *Sesbania grandiflora* in cigarette smoke-exposed rats. Journal of Cardiovascular Pharmacology 52 (4), 338–343.

Ramesh, T., Sureka, C., Bhuvana, S., Begum, V.H., 2015. Brain oxidative damage restored by *Sesbania grandiflora* in cigarette smoke-exposed rats. Metabolic Brain Disease 30 (4), 959–968.

Ramesh, T., Sureka, C., Bhuvana, S., Begum, V.H., 2010. *Sesbania grandiflora* diminishes oxidative stress and ameliorates antioxidant capacity in liver and kidney of rats exposed to cigarette smoke. Journal of Physiology and Pharmacology 61 (4), 467–476.

Sarian, M.N., Ahmed, Q.U., Mat So'ad, S.Z., Alhassan, A.M., Murugesu, S., Perumal, V., et al., 2017. antioxidant and antidiabetic effects of flavonoids: A structure-activity relationship-based study. Biomed Research International. 2017. https://doi.org/10.1155/2017/8386065. article 8386065.

Šarić Mustapić, D., Debeljak, Ž., Maleš, Ž., Bojić, M., 2018. The inhibitory effect of flavonoid aglycones on the metabolic activity of CYP3A4 enzyme. Molecules 23 (10), 2553.

Sathasivampillai, S.V., Rajamanoharan, P.R., Heinrich, M., 2018. Siddha medicine in eastern sri lanka today−Continuity and change in the treatment of diabetes. Frontiers in Pharmacology 9. https://doi.org/10.3389/fphar.2018.01022.

Sato, N., Li, W., Tsubaki, M., Higai, K., Takemoto, M., Sasaki, T., Onoda, T., et al., 2017. Flavonoid glycosides from japanese *camellia* oil cakes and their inhibitory activraity against advanced glycation end-products formation. Journal of Functional Foods 35, 159–165.

Sang, S., Cheng, X., Zhu, N., Stark, R.E., Badmaev, V., Ghai, G., et al., 2001. Flavonol glycosides and novel iridoid glycoside from the leaves of *Morinda citrifolia*. Journal of Agricultural Food Chemistry 49 (9), 4478–4481.

Shareef, H., Rizwani, G.H., Zia-ul-Haq, M., Ahmad, S., Zahid, H., 2012. Tocopherol and phytosterol profile of *Sesbania grandiflora* (Linn.) seed oil. Journal of Medicinal Plant Research 6 (18), 3478–3481.

Shakeel, U., Inamullah, F., Fatima, I., Khan, S., Kazmi, M.H., Malik, A., et al., 2016. Colutin, new antifungal isoflavan from *Colutea armata*. Chemistry of Natural Compounds 52 (4), 611–614.

Shimizu, S., Miyase, T., Ueno, A., Usmanghani, K., 1989. Sesquiterpene lactone glycosides and ionone derivative glycosides from *Sonchus asper*. Phytochemistry 28 (12), 3399–3402.

Sureka, C., Ramesh, T., Begum, V.H., 2015. Attenuation of erythrocyte membrane oxidative stress by *Sesbania grandiflora* in streptozotocin-induced diabetic rats. Biochemistry and Cell Biology 93 (4), 385–395.

Talapatra, S.K., Talapatra, B., 2015. Chemistry of Plant Natural Products. Spriger.

Thompson, J.D., Higgins, D.G., Gibson, T.J., 1994. CLUSTAL W: improving the sensitivity of progressive multiple sequence alignment through sequence weighting, position-specific gap penalties and weight matrix choice. Nucleic Acids Research 22, 4673–4680.

Villa−Rodriguez, J.A., Aydin, E., Gauer, J.S., Pyner, A., Williamson, G., Kerimi, A., 2017. Green and chamomile teas, but not acarbose, attenuate glucose and fructose transport via inhibition of GLUT2 and GLUT5. Molecular Nutrition and Food Research 61 (12), 1700566.

Visvanathan, R., Jayathilake, C., Liyanage, R., 2016. A simple microplate-based method for the determination of α-amylase activity using the glucose assay kit (GOD method). Food Chemistry 211, 853–859.

Vinayagam, R., Xu, B., 2015. Antidiabetic properties of dietary flavonoids: a cellular mechanism review. Nutrition and Metabolism 12 (1), 60.

Wang, S., Xu, Y., Jiang, W., Zhang, Y., 2013. Isolation and identification of constituents with activity of inhibiting nitric oxide production in raw 264.7 macrophages from *gentiana triflora*. Planta Medica 79 (08), 680–686.

Visvanathan, R., Jayathilake, C., Liyanage, R., Sivakanesan, R., 2019. Applicability and reliability of the glucose oxidase method in assessing α-amylase activity. Food Chemistry 275, 265–272.

Wagh, V.D., Wagh, K.V., Tandale, Y.N., Salve, S.A., 2009. Phytochemical, pharmacological and phytopharmaceutics aspects of *Sesbania grandiflora* (Hadga): a review. Journal of Pharmaceutical Research 2 (5), 889–892.

Waterhouse, A., Bertoni, M., Bienert, S., Studer, G., Tauriello, G., Gumienny, R., et al., 2018. . SWISS-MODEL: homology modelling of protein structures and complexes. Nucleic Acids Research 46 (W1), W296–W303.

Wei, Y., Xie, Q., Fisher, D., Sutherland, I.A., 2011. Separation of patuletin-3-O-glucoside, astragalin, quercetin, kaempferol and isorhamnetin from *flaveria bidentis* (L.) kuntze by elution-pump-out high-performance counter-current chromatography. Journal of Chromatography. A 1218 (36), 6206–6211.

Whazin, K.A., Gatilov, Y.B., Adekenev, S.M., 1995. Gaigranin and gaigrandin—New sesquiterpene lactones from *Gaillardia grandiflora*. Chemistry of Natural Compounds 31 (1), 63–67.
Whitcomb, D.C., Lowe, M.E., 2007. Human pancreatic digestive enzymes. Digestive Diseases and Sciences 52 (1), 1–17.
Williams, L.K., Li, C., Withers, S.G., Brayer, G.D., 2012. Order and disorder: differential structural impacts of myricetin and ethyl caffeate on human amylase, an antidiabetic target. Journal of Medicinal Chemistry 55 (22), 10177–10186.
Xiao, Z., Storms, R., Tsang, A., 2006. A quantitative starch? iodine method for measuring alpha-amylase and glucoamylase activities. Analytical Biochemistry 351 (1), 146–148.
Xu, L., Patrick, B.O., Roberge, M., Allen, T., van Ofwegen, L., Andersen, R.J., 2000. New diterpenoids from the octocoral *pachyclavularia violacea* collected in papua new guinea. Tetrahedron 56 (46), 9031–9037.
Yang, Z., Nakabayashi, R., Mori, T., Takamatsu, S., Kitanaka, S., Saito, K., 2016. Metabolome analysis of *oryza sativa* (rice) using liquid chromatography-mass spectrometry for characterizing organ specificity of flavonoids with anti-inflammatory and anti-oxidant activity. Chemical and Pharmaceutical Bulletin 64 (7), 952–956.
Zamroni, A., Widjanarko, S.B., Rifa'i, M., Zubaidah, E., 2017. Antihyperglycemic effect of *Sesbania grandiflora* seed decoction on streptozotocin-induced diabetic mice: inflammatory status and the role of interleukin-10. In: Proceedings of the AIP Conference Proceedings. 1844, AIP Publishing, 020015.
Zhou, Z.L., Yin, W.Q., Zou, X.P., Huang, D.Y., Zhou, C.L., Li, L.M., et al., 2014. Flavonoid glycosides and potential antivirus activity of isolated compounds from the leaves of *Eucalyptus citriodora*. Journal of the Korean Society for the Applied Biological Chemistry 57 (6), 813–817.